ORIGINAL ARTICLE

TBC1D15 deficiency protects against doxorubicin cardiotoxicity *via* inhibiting DNA-PKcs cytosolic retention and DNA damage

Wenjun Yu[a,b,c,d,†], Haixia Xu[a,b,e,†], Zhe Sun[a,b,†], Yuxin Du[a,b,†], Shiqun Sun[a,b], Miyesaier Abudureyimu[b,f], Mengjiao Zhang[a,b], Jun Tao[g], Junbo Ge[a,b], Jun Ren[a,b,*], Yingmei Zhang[a,b,*]

[a]Department of Cardiology and Shanghai Institute of Cardiovascular Diseases, Zhongshan Hospital, Fudan University, Shanghai 200032, China
[b]National Clinical Research Center for Interventional Medicine, Shanghai 200032, China
[c]Department of Cardiovascular Surgery, Zhongnan Hospital of Wuhan University, Wuhan 430071, China
[d]Hubei Provincial Engineering Research Center of Minimally Invasive Cardiovascular Surgery, Wuhan 430071, China
[e]Department of Cardiology, Affiliated Hospital of Nantong University, Nantong 226001, China
[f]Cardiovascular Department, Shanghai Xuhui Central Hospital, Zhongshan-Xuhui Hospital, Fudan University, Shanghai 200030, China
[g]Department of Cardiovascular Surgery, Sun Yat-sen Memorial Hospital, Sun Yat-sen University, Guangzhou 510000, China

Abstract Clinical application of doxorubicin (DOX) is heavily hindered by DOX cardiotoxicity. Several theories were postulated for DOX cardiotoxicity including DNA damage and DNA damage response (DDR), although the mechanism(s) involved remains to be elucidated. This study evaluated the potential role of TBC domain family member 15 (TBC1D15) in DOX cardiotoxicity. Tamoxifen-induced cardiac-specific *Tbc1d15* knockout (*Tbc1d15*[CKO]) or *Tbc1d15* knockin (*Tbc1d15*[CKI]) male mice were challenged with a single dose of DOX prior to cardiac assessment 1 week or 4 weeks following DOX challenge. Adenoviruses encoding TBC1D15 or containing shRNA targeting *Tbc1d15* were used for *Tbc1d15* overexpression or knockdown in isolated primary mouse cardiomyocytes. Our results revealed that DOX evoked upregulation of TBC1D15 with compromised myocardial function and overt mortality, the effects of which were ameliorated and accentuated by *Tbc1d15* deletion and *Tbc1d15*

*Corresponding authors. Tel.: +86 21 64041990 (Yingmei Zhang); +86 21 64223006 (Jun Ren).
E-mail addresses: zhangym197951@126.com (Yingmei Zhang), jren_aldh2@outlook.com (Jun Ren).
†These authors made equal contributions to this work.

overexpression, respectively. DOX overtly evoked apoptotic cell death, the effect of which was alleviated and exacerbated by *Tbc1d15* knockout and overexpression, respectively. Meanwhile, DOX provoked mitochondrial membrane potential collapse, oxidative stress and DNA damage, the effects of which were mitigated and exacerbated by *Tbc1d15* knockdown and overexpression, respectively. Further scrutiny revealed that TBC1D15 fostered cytosolic accumulation of the cardinal DDR element DNA-dependent protein kinase catalytic subunit (DNA-PKcs). Liquid chromatography—tandem mass spectrometry and co-immunoprecipitation denoted an interaction between TBC1D15 and DNA-PKcs at the segment 594−624 of TBC1D15. Moreover, overexpression of TBC1D15 mutant (Δ594−624, deletion of segment 594−624) failed to elicit accentuation of DOX-induced cytosolic retention of DNA-PKcs, DNA damage and cardiomyocyte apoptosis by TBC1D15 wild type. However, *Tbc1d15* deletion ameliorated DOX-induced cardiomyocyte contractile anomalies, apoptosis, mitochondrial anomalies, DNA damage and cytosolic DNA-PKcs accumulation, which were canceled off by DNA-PKcs inhibition or ATM activation. Taken together, our findings denoted a pivotal role for TBC1D15 in DOX-induced DNA damage, mitochondrial injury, and apoptosis possibly through binding with DNA-PKcs and thus gate-keeping its cytosolic retention, a route to accentuation of cardiac contractile dysfunction in DOX-induced cardiotoxicity.

1. Introduction

Doxorubicin (DOX) is one of the most widely employed chemotherapeutic drugs for the clinical treatment of solid and hematogenous malignancies[1,2]. Unfortunately, the clinical application of DOX has been largely hindered due to its cumulative toxicity in nontumor cells, especially cardiomyocytes[3−5]. Sustained DOX exposure triggers a unique form of cardiomyopathy encompassing histopathological and functional anomalies, characterized by overt pathological changes including arrhythmia, left ventricular dysfunction and congestive heart failure reminiscent of dilated cardiomyopathy (DCM)[6]. To date, a plethora of mechanisms are postulated for the onset and development of DOX-induced cardiotoxicity including DNA damage[7,8], transcriptome aberrations[9], oxidative stress[10,11], mitochondrial iron accumulation[12], inflammation[13] and autophagy derangement[14]. In particular, ample evidence recently noted a vital role for DNA damage in DOX-induced cardiotoxicity[15−17]. DNA damage is generally evoked by stresses including drug usage, radiation exposure and oxidative stress, all of which turn on DNA damage response (DDR)[18]. DOX challenge elicited DNA damage, ataxia-telangiectasia-mutated (ATM) activation, and p53 accumulation in the heart[19]. This is in line with the findings of suppressed myocardial apoptosis using pharmacological inhibition or genetic ablation of p53 in the face of DOX challenge[20]. Once activated, DDR elicits undesired myocardial responses, coinciding with an earlier finding where DDR inhibition alleviates DOX-induced cardiotoxicity[21]. In this context, it is pertinent to identify the regulatory mechanisms for DDR in an effort to best manage DOX-induced cardiotoxicity.

Among various regulatory elements elaborated for DDR[22], a member of the phosphatidylinositol 3-kinase-related family of protein kinases—DNA-dependent protein kinase catalytic subunit (DNA-PKcs), received much recent attention in stress conditions including aging[23], radiation[24], oxidative stress[25], asthma[26] and type 2 diabetes mellitus[27]. DNA-PKcs is a canonical molecule to initiate DNA double-strand repair in the face of overwhelmed DNA damage[28]. Intriguingly, DNA-PKcs-mediated DNA repair machinery was reported to offer a beneficial role in DOX-induced cardiotoxicity[19]. Under physiological condition, intranuclear DNA-PKcs primarily binds to Ku80[28], which functions as an intrinsic repair element to revamp DNA by recognizing and interacting with the broken segments of DNA. Levels of DNA-PKcs were found elevated in failing human hearts although the underlying mechanism remains unclear[29]. Meanwhile, phosphorylation of DNA-PKcs was turned on in response to cardiac oxidative ischemia/reperfusion injury based on our recent finding, where loss of DNA-PKcs protects against oxidative damage in cardiac ischemia/reperfusion injury[30]. This finding denotes distinct cellular roles for DNA-PKcs depending on the location and state of the enzyme.

TBC domain family member 15 (TBC1D15), a ubiquitously expressed protein belonging to the Tre-2/Bub2/Cdc16, functions as a GTPase-activating protein for RAB7 and RAB11[31]. Recent studies revealed that GTP-bound RAB7 mediates mitochondria-lysosome contacts formation while TBC1D15 promotes contacts untethering between mitochondria and lysosomes in mammalian cells, leading to the regulation of mitochondrial dynamics and metabolites or ion transfer between two organelles[32,33]. Further finding from our group revealed that *Tbc1d15* overexpression alleviates cardiac injury following myocardial infarction or myocardial ischemia—reperfusion by preserving mitochondrial function[34,35]. TBC1D15 was reported to regulate DNA-sensing[36]. Nonetheless, the role for TBC1D15 in DOX-induced cardiotoxicity and possible involvement of DNA damage/repair remains at large. Herein, this study was designed to examine the role of TBC1D15 in DOX-induced cardiotoxicity and the underlying mechanism(s) involved with a focus on DNA-PKcs-regulated DNA damage.

2. Methods

2.1. Animal models and human samples

All animal procedures were performed in accordance with the Guide for the Care and Use of Laboratory Animals (National Institutes of Health Publication No. 85−23), and were approved by the Animal Use and Care Committee of Zhongshan Hospital, Fudan University (Shanghai, China). Experimental procedures

involving human samples were approved by the institutional ethics committee of Sun Yat-sen Memorial Hospital, Sun Yat-sen University, Guangzhou, China (SYSEC-KY-KS-2019-019). In brief, human heart samples were obtained from patients with dilated cardiomyopathy (DCM) for heart transplantation from Sun Yat-sen Memorial Hospital, Sun Yat-sen University. Donor hearts not meeting transplantation criteria due to technical reasons were employed as controls.

Genetically-engineered mice were generated by the Cyagen Biosciences (Suzhou, China) using well-established CRISPR/Cas9-mediated genome engineering as described previously[34]. Briefly, cardiomyocyte Tbc1d15 (NM_025706, chromosome 10) conditional knockout (Tbc1d15^CKO) mice were generated using the Tbc1d15^flox/flox mice bred with the Myh6-Cre transgenic mice. The Myh6-Cre transgenic mice contained the mouse cardiac-specific alpha-myosin heavy chain promoter directing expression of a tamoxifen-inducible Cre recombinase to cardiomyocytes, which resulted in deletion of loxP-flanked targeted genes in cardiac tissues. Exon 4 of Tbc1d15 gene was selected as the conditional knockout region, which was flanked with loxP sites in vivo. In consideration of negative effects by tamoxifen-inducible Cre expression on mouse cardiac function and morphology, easily accessible Cre-negative mice (Tbc1d15^flox/flox) from littermates of genetically-engineered mice were employed as wild type controls instead of Cre-positive mice (Myh6-Cre)[37]. Target gene manipulation was induced by intraperitoneal injection of tamoxifen (T5648, Sigma−Aldrich, St. Louis, MO, USA) at a dosage of 40 mg/kg for 3 doses on alternate days[38]. Control mice (Tbc1d15^flox/flox) received same dosage of tamoxifen. This dosage of tamoxifen was adopted as low to intermediate levels of tamoxifen or its metabolites have proven to exert little unwanted side effects on cardiac function, energetics or fibrosis in adult mice generated by the αMHC-Mer-CreMer/loxP system[39]. For the TBC1D15 gain-of-function study, cardiomyocyte Tbc1d15 (NM_025706.3, chromosome 10) conditional knockin (Tbc1d15^CKI) mice were generated using the "CAG-loxP-Stop-loxP-Kozak-mouse Tbc1d15 CDS-polyA" cassette which was cloned into intron 1 of Rosa26 (NR_027008.1, chromosome 6) and were then bred with Myh6-cre transgenic mice in a tamoxifen-dependent manner. Littermates were used as wild-type controls. All mice were backcrossed on a C57BL/6 N background for at least three generations and were reared with enough sterilized water and food following a 12/12 circadian cycle. To rule out potential sex-related variation as estrogen levels in female mice may interfere the effect of tamoxifen-induced conditional knockout or knockin on cardiac-specific Tbc1d15 knockout or Tbc1d15 knockin mice, only adult male mice (8−12 weeks) were used in all experiments. Two weeks following tamoxifen injection, mice were challenged with doxorubicin (DOX) (D1515, Sigma−Aldrich, 12.5 mg/kg, dissolved in saline, single intraperitoneal injection) for 1 week or 4 weeks as described previously[40] with minor modification of the dosage. Same volume of saline was used as control.

2.2. Isolation, cell culture and DOX challenge in adult and neonatal cardiomyocytes

Neonatal mouse cardiomyocytes (NMCMs) were isolated and cultured according to our previously described protocols[41]. Briefly, hearts from sterilized neonatal mice (one day old) were quickly excised and digested in type I collagenase (LS004194, Worthington, Lakewood, NJ, USA) for several minutes at each time. After differentially pre-plating for 90 min to remove

fibroblasts, NMCMs were replanted onto gelatin-coated culture plates at approximately 2×10^5 cells per cm^2 and were incubated with a complete Dulbecco's modified Eagle's medium (11995073, DMEM, Gibco, Grand Island, NY, USA) containing 10% fetal bovine serum (10099141, FBS, Gibco) and 1% penicillin/streptomycin mixture (10378016, Gibco) in an incubator (Thermo Fisher Scientific, Waltham, MA, USA) at 37 °C, 95% air, 5% CO$_2$ for 48 h. Brdu (5-bromo-2′-deoxyuridine) was used to inhibit the growth of fibroblasts.

Adult mouse cardiomyocytes (AMCMs) were isolated and cultured as described[42,43]. In brief, mice were anesthetized and the heart was exposed. An ethylene diamine tetraacetic acid (EDTA, Gibco) buffer was infused into the right ventricle. Ascending aorta were tightly clamped prior to the excision of the heart. EDTA and perfusion buffers were sequentially injected into left ventricles before a collagenase buffer (type II and IV, LS004174 and LS004186, Worthington). Following separation, left ventricles were gently cut into 1-mm^3 pieces and were dissociated using gentle pipetting. Cell suspension was then undergone four sequential rounds of gravity settling, prior to Ca^{2+} replenishment. A yield of at least 80% rod-shaped cardiomyocytes was deemed successful. NMCMs and AMCMs were challenged with the indicated concentration of DOX (dissolved in dimethyl sulfoxide) for 24 h.

2.3. Cardiomyocytes transfection

Short hairpin RNA (shRNA) against negative control or Tbc1d15 and small interfering RNA (siRNA) against negative control, Rab7 or Rab11 were obtained from the Genechem Corporation (Shanghai, China) with target sequences as follows: sh-Tbc1d15: 5′-GCCAAAGATGACAGTCCAA-3′; si-Rab7: 5′-CCAGA-CAAUUGCUCGGAAUTT-3′; si-Rab11: 5′-GGCAGUUCCUA-CAGAUGAATT-3′. Adenoviruses encoding TBC1D15 (wild type, shRNA) were produced by the Obio Technology Corporation (Shanghai, China). Plasmids encoding TBC1D15 (wild type, Δ280−320, Δ476−506, Δ594−624) and adenovirus encoding (Δ594−624) were purchased from Hanbio Biotechnology (Shanghai, China)[35]. An adenoviral vector encoding β-galactosidase was used as the control.

Adenoviral transfection was described[35]. Briefly, 48 h after plating, cardiomyocytes were transfected with adenovirus encoding TBC1D15 (wild type, shRNA or Δ594−624) at MOI of 10 for 2 h, neutralized with FBS for 22 h and then refreshed with DMEM (with or without DOX) for another 24 h. The efficiency of transfection with adenovirus was verified using Western blot. Thereafter, NMCMs were stimulated with 3 μmol/L DOX while AMCMs were challenged with 1 μmol/L DOX, as higher concentration of DOX could result in visible loss of cardiomyocyte contractile capacity and severe cell death. The protocol of plasmid transfection or siRNA knockdown was described in our previous report[44].

2.4. RNA-sequencing data analysis

RNA-sequencing data (GSE120895, 8 non-dilated and 47 dilated cardiomyopathy patients) were downloaded from the gene expression omnibus (http://www.ncbi.nlm.nih.gov/geo) database. The "limma" R package (version 3.32.3) was applied to process the gene expression data (R version 4.1.0). Differential expression of TBC1D15, NPPA and NPPB between non-dilated and dilated cardiomyopathy patients was analyzed using Student's t-test.

Gene set enrichment analysis for the single gene based on the kyoto encyclopedia of genes and genomes was used to explore the pathways related to TBC1D15. First, 47 dilated cardiomyopathy patients were divided into low and high *TBC1D15* groups according to the median value of *TBC1D15*. Then, gene set enrichment analysis software (version 4.1.0) was used to enrich significant pathways correlated with these two groups. The source code was shown in supplemental materials and its R Markdown format could be downloaded as well.

2.5. Immunohistochemistry

Heart tissues were fixed in 4% paraformaldehyde, embedded in paraffin and were then cut into 5-μm sections. Sections were deparaffinized prior to rehydration. Following antigen retrieval, sections were blocked with 5% bovine serum albumin, incubated with anti-TBC1D15 primary antibody (1:50, Abcam, Cambridge, MA, ab121396) at 4 °C overnight and were then incubated with a horseradish secondary antibody (1:200) at room temperature. Following incubation with diaminobenzidine, sections were counterstained with hematoxylin. Images were captured using a 40 × objective under a Leica microscope (Heidelberg, Germany). Percentage of positive stained area was calculated using the Image J software (National Institute of Health, Version 1.8). Six to seven fields per section and 6 heart tissues per group were used for analysis.

2.6. Cardiomyocyte cross-sectional area detection

Cardiomyocyte cross-sectional area was detected using wheat germ agglutinin (L4895, WGA, Sigma−Aldrich) staining[45]. Briefly, hearts from anesthetized mice were immediately excised and fixed in 4% paraformaldehyde at room temperature for 24 h. Specimens were embedded in paraffin, cut into 5-μm sections and stained with fluorescein isothiocyanate-conjugated WGA. Images were taken using a Leica microscopy at 40 × objective. Six fields per heart and 6 mice per group were collected. Images were segmented with cellpose, and then cardiomyocyte cross-sectional areas in each field were assessed using the Image J software *via* the LabelsToROIs modality[46]. Incomplete cells on the edges of each image or not displaying cross-sectioning (with too high or too low circularity indices) were excluded. The average area of cardiomyocytes from all fields of each heart was calculated.

2.7. Echocardiographic measurement

Myocardial geometry and function were assessed using a 2-D guided M-mode echocardiography (Vevo 2100, Fujifilm Visual Sonics, Toronto, ON, Canada) equipped with an 18-MHz linear transducer (MS400, Fujifilm Visual Sonics)[41]. Mice were anesthetized by 2% isoflurane inhalation and hearts were imaged in the 2-D mode through the parasternal short-axis view prior to M-mode. Left ventricular end-diastolic and end-systolic dimensions (LVEDD, LVESD) were measured. Interventricular septum thickness (IVS) and left ventricular posterior wall thickness (LVPW) were obtained at the time of the apparent maximal diastolic diameter. Heart rate was obtained by simultaneous electrocardiogram examination. Left ventricular end-diastolic and end-systolic volumes (LVEDV, LVESV), fractional shortening (FS) and ejection fraction (EF) were calculated using Vevo 2100 software. FS was calculated as Eq. (1) and EF was obtained from Eq. (2):

$$FS\,(\%) = (LVEDD - LVESD)/LVEDD \times 100 \tag{1}$$

$$EF\,(\%) = (LVEDV - LVESV)/LVEDV \times 100 \tag{2}$$

2.8. Shortening/relengthening

Mechanical properties of cardiomyocytes were monitored using a Softedge MyoCam system (IonOptix, Milton, MA, USA) equipped with an IX-70 Olympus inverted microscope[47]. Contractile buffer (NaCl 135 mmol/L, KCl 4.0 mmol/L, CaCl$_2$ 1.0 mmol/L, MgCl$_2$ 1.0 mmol/L, glucose 10 mmol/L and HEPES 10 mmol/L) was added and cells were electrically challenged at the frequency of 0.5 Hz. Cell shortening and relengthening were assessed using the following indices including peak shortening (PS), maximal velocity of shortening ($+\mathrm{d}L/\mathrm{d}t$), maximal velocity of relengthening ($-\mathrm{d}L/\mathrm{d}t$), time-to-PS (TPS), and time-to-90% relengthening (TR$_{90}$).

2.9. Cardiomyocyte apoptosis assessment

Terminal deoxynucleotidyl transferase-mediated dUTP nick end labeling (TUNEL) assay was adopted to evaluate myocardial apoptosis using an In Situ Cell Death Detection Kit (11684795910, Roche, Basel, Switzerland) according to the manufacturer's manual. For animal study, 2 images per heart and 4 to 5 mice per group were taken using a Leica microscopy at 40 × objective. For cell study, 5 to 15 images from 3 independent isolations were obtained. At least 100 cells per group were counted. Numbers of TUNEL-positive nuclei and DAPI-stained nuclei were counted using Image J. Apoptosis was evaluated as the percentage of TUNEL-positive nuclei to that of total nuclei.

2.10. Western blot

As described previously[48], protein samples were collected using a radio immunoprecipitation assay buffer (P0013B, Beyotime Biotechnology, Shanghai, China) containing phosphatase and protease inhibitor (P1045, Beyotime Biotechnology). Equal quantities (20 μg) of proteins were separated by 10%−12% SDS-PAGE (P0012A, Beyotime Biotechnology), and then electrophoretic transferred to 0.22 μm PVDF membranes (GVWP02500, Merck Millipore, Billerica, MA, USA). After blocking with 5% non-fat milk in Tris-buffer-solution containing Tween-20 (TBST) buffer (P0233, Beyotime Biotechnology) for 60 min, membranes were incubated with selective primary antibodies overnight at 4 °C. Blots were rinsed three times for 10 min in TBST and were incubated with horseradish peroxidase-conjugated secondary antibody for 2 h at room temperature. Densitometry was detected with enhanced ECL reagent (1705061, Bio-Rad Laboratories, Hercules, CA, USA) using a Bio-Rad detector. All antibodies used for Western blot are shown in Supporting Information Table S1.

2.11. Real-time polymerase chain reaction (real-time PCR)

Total RNA of hearts was isolated using the TRIzol reagent and a RNeasy Total RNA Isolation Kit (12866-25, Qiagen, Hilden, Germany), and was then reverse-transcribed using an iScript cDNA Synthesis Kit (6130, Takara BIO, Otsu, Japan). Real-time PCR was performed using iQ SYBR Green Supermix (1708882, Bio-Rad Laboratories) in the CFX96 Touch Real-Time PCR Detection System (Bio-Rad Laboratories). All primers employed for real-time PCR are shown in Supporting Information Table S2.

2.12. Enzyme-linked immunosorbent assay (ELISA)

Serum levels of biomarkers including lactate dehydrogenase (LDH), creatine kinase-MB (CKMB) and cardiac troponin-T (cTnT) were detected in mice using commercial assay kits of LDH, CKMB and cTnT, respectively (A020-2-2, H197-1-2, H149-4, Nanjing Jincheng Bioengineering Institute, Nanjing, China). Levels of reduced glutathione (GSH) and oxidized glutathione (GSSG) were detected using the GSH and GSSG Assay Kit (S0053, Beyotime, China).

2.13. DNA damage detection

Histone H2A.X is phosphorylated on Ser139, termed gamma H2A.X (γH2A.X), in the setting of DNA damage[49]. γH2A.X is regarded as the marker of DNA damage[50]. To assess DNA damage in cardiomyocytes, cells fixed with 4% paraformaldehyde were stained with an antibody against γH2A.X (1:50) at 4 °C overnight alongside the relevant fluorescent secondary antibody (1:200).

2.14. Transmission electron microscopy (TEM)

TEM ultrastructural examination was performed as described[35]. Briefly, murine heart tissues were fixed, immersed and polymerized. Sections (75−80 nm) were cut and collected on 200-mesh copper grids. After poststained, sections were observed using a 40−120 kV transmission electron microscope (Hitachi H600 Electron Microscope, Hitachi, Japan). Approximately ten microscopic fields from 3 hearts per group were analyzed. For mitochondrial morphology analysis, number of normal or damaged mitochondria within a field of 150 μm^2 was counted with the assistance of Image J. Mitochondrial size including major or minor axis length was measured using the Multi measure ROI tool of Image J. Mitochondrial circularity index was derived from minor axis length/major axis length. For autophagosome analysis, autophagosomes (characterized by double-membrane sequestering vesicles containing damaged mitochondria or protein aggregates) were manually counted.

2.15. Assessment of mitochondrial function

Mitochondrial membrane potential was examined using tetramethylrhodamine methyl ester (TMRM) (I34361, Thermo Fisher Scientific). Mitochondrial reactive oxygen species production was measured with 2′,7′-dichlorofuorescein-diacetate (S0033S, DCFH-DA, Beyotime Biotechnology) and mitoSOX (M36008, Thermo Fisher Scientific). A laser confocal microscope (Leica) was used to observe the fluorescence.

2.16. Immunofluorescence

For immunofluorescence, NMCMs were fixed with 4% paraformaldehyde for 15 min at room temperature. After permeabilizing in phosphate buffered saline containing 0.2% Triton X-100 and 5% FBS for 1 h, NMCMs were incubated with primary antibodies overnight at 4 °C. After rinsing with phosphate buffered saline, NMCMs were incubated with Alexa Fluor-conjugated secondary antibodies. Following staining, immunofluorescence of NMCMs was examined using a Leica laser confocal microscope with a 63× oil objective at the indicated excitation wavelength. All antibodies used for immunofluorescence are included in Supporting Information Table S3.

2.17. Fractional protein extraction

Nuclear and cytoplasmic proteins were isolated using a Nuclear and Cytoplasmic Protein Extraction Kit (P0027, Beyotime Biotechnology) per the manufacturer's instruction. Briefly, tissues were cut into fine pieces, and tissue homogenate solution containing reagent A and B (20:1, PMSF 1 mmol/L) were added. Tissues were homogenized at 4 °C for 15 min and were centrifuged at $1500 \times g$ for 15 min (4 °C). The supernatant was collected (cytosolic protein lysate). The remaining precipitate was continually mixed with reagent A (200 μL:20 μL, PMSF 1 mmol/L) and vortexed for 5 s. After 10−15 min on ice, reagent B (10 μL, PMSF 1 mmol/L) was added prior to vortexing for 5 s. Following a 1-min incubation on ice, tissues were centrifuged at $15,000 \times g$ for 5 min (4 °C) and supernatant (cytosolic protein lysate) was collected. The remaining precipitate was mixed with reagent C (50 μL, PMSF 1 mmol/L) and was vortexed for 15−30 times (15−30 s per time). Tissues were centrifuged at $15,000 \times g$ for 10 min (4 °C) and the supernatant was collected as the nuclear protein lysate.

2.18. Immunopurification and mass spectrometry (IP/MS)

NMCMs were transfected with TBC1D15-Flag adenovirus. Cell lysates were immunoprecipitated using the anti-Flag magnetic beads 48 h following transfection. Precipitates were separated by SDS-PAGE and were subsequently stained with Coomassie blue (P0017F, Beyotime Biotechnology). Stained protein bands were cut into small pieces and were digested for peptide extraction. Liquid chromatography−tandem mass spectrometry was applied for proteomic data analysis with the extracted peptides. Top 5 of TBC1D15-interacting proteins identified by IP/MS are shown in Supporting Information Table S4.

2.19. Immunoprecipitation

Cells transiently overexpressing Flag-tagged genes were treated in a lysis buffer containing 50 mmol/L Tris−HCl (pH 7.5), 150 mmol/L NaCl, protease inhibitor cocktails and NP-40 (P0013F, Beyotime Biotechnology). After centrifugation, supernatant fractions were subjected to immunoprecipitation with monoclonal IgG (1:1000, 3423, Cell Signaling) and monoclonal Flag antibodies (1:500, 70569, Sigma−Aldrich) incubated on protein-A/G beads (LSKMAGAG, Sigma−Aldrich). Precipitants were analyzed using SDS-PAGE and subsequently immunoblotting.

2.20. Structure-based protein interaction interface analysis between TBC1D15 and DNA-PKcs

Protein structures of TBC1D15 (NCBI reference sequence: NP_079982.3) were further predicted by template-based homology structure modeling tool SWISS-MODEL (https://www.swissmodel.expasy.org), using PDB structure 5TUC, chain A (covering residues 284−614, sequence identity = 94.83%) and 5TUB, chain A (covering residues 280−614, sequence identity = 77.81%) as the templates, respectively. Structures of DNA-PKcs (GenBank: BAA28875) were predicted using PDB structure 5LUQ, chain A (covering residues 10−4127, sequence identity = 75.91%), 5Y3R, chain F (covering residues 10−4128, sequence identity = 79.35%) and 5WLR, chain A (covering residues 8−4127, sequence identity = 79.33%) as the templates. Then, the protein−protein interaction was docked and modeled using the PRISM 2.0 server (http://cosbi.ku.edu.tr/prism) to

predict their potential interaction interface. Prediction result containing docking structure with the lowest energy score are shown in Supporting Information Table S5 and further visualized using the PyMol tool (V2.4.0, http://www.pymol.org/).

2.21. Statistical analysis

All data were expressed as mean ± standard error of the mean (SEM). Data were analyzed using GraphPad Prism 9 (GraphPad Software, LLC, San Diego, CA, USA). The Kaplan−Meier survival curve was analyzed using the Gehan-Breslow-Wilcoxon test. Normality of data distribution was examined using the Shapiro−Wilk normality test. Two group comparison was performed using Student's *t*-test (two-tailed). Multiple groups were compared using one-way or two-way ANOVA followed by the Tukey *post hoc* test. A value of $P < 0.05$ was considered statistically significant.

3. Results

3.1. Effect of doxorubicin challenge on TBC1D15 levels in cardiac tissues and cardiomyocytes

RNA-sequencing data (GSE120895) from 8 non-dilated and 47 dilated cardiomyopathy (DCM) patients were downloaded from the gene expression omnibus and were analyzed using R package. Gene set enrichment analysis for the single gene based on the kyoto encyclopedia of genes and genomes database suggested higher *TBC1D15* gene levels along with increased levels of heart failure indicators including *NPPA* (atrial natriuretic peptide, ANP) and *NPPB* (type B natriuretic peptide, BNP) in heart tissues from DCM patients compared with those from non-dilated controls (Supporting Information Fig. S1A). Then, 47 DCM patients were divided into low and high *TBC1D15* groups according to the median value of *TBC1D15*. Further analysis showed that higher *TBC1D15* expression was obviously enriched with numerous processes especially in non-homologous end joining (Fig. S1B). Since it is impractical to collect heart samples from patients suffering from doxorubicin (DOX) toxicity in heart transplantation, there are no appropriate DOX cardiomyopathy samples from human. Given that DOX challenge can trigger DCM, DCM human samples were used instead. Clinical information of 6 DCM patients and 6 controls are shown in Supporting Information Table S6. Protein levels of TBC1D15 were deciphered in heart tissues from DCM patients using Western blot and immunohistochemistry. Along the same line, TBC1D15 levels were dramatically increased in DCM heart tissues in conjunction with elevated BNP levels from patients with DCM (Fig. S1C−S1E). Immunohistochemistry also validated an obvious rise in TBC1D15 intensity in heart slices from DCM patients (Fig. S1F and S1G). To evaluate the effect of DOX on TBC1D15 levels *in vivo*, mice were challenged with DOX (12.5 mg/kg). Our data revealed that TBC1D15 levels were significantly upregulated 7 days following DOX challenge (Fig. 1A and B). Ample evidence has indicated an essential role for DNA damage in DOX-induced cardiotoxicity[15−17]. We monitored DNA damage using its protein marker histone H2A.X phosphorylation at Ser[139], termed gamma H2A.X (γH2A.X)[19]. Ratio of γH2A.X to H2A.X was overtly increased in mouse heart tissues challenged with DOX (Fig. 1C). To assess the possible relationship between TBC1D15 and DOX-induced DNA damage, neonatal mouse cardiomyocytes (NMCMs)

were challenged with DOX for 24 h at indicated concentrations (0, 0.5, 1, and 3 µmol/L) prior to assessment of TBC1D15 using Western blot and DNA damage using γH2A.X immunofluorescence. Our data revealed an overt rise for TBC1D15 at protein level in cardiomyocytes in a dose-dependent manner following 24-h DOX exposure, in parallel with changes of γH2A.X immunofluorescence intensity (Fig. 1D−F).

3.2. Effect of TBC1D15 on DOX-induced changes in myocardial function and morphology

To discern the effect of TBC1D15 on DOX cardiotoxicity, tamoxifen-induced cardiac-specific *Tbc1d15* knockout (*Tbc1d15*CKO) or knockin (*Tbc1d15*CKI) mice were generated for loss- or gain-of-function examination (Supporting Information Fig. S2, Fig. 2A and Supporting Information Fig. S4A). The efficiency of cardiac-specific *Tbc1d15* knockout or knockin in isolated adult mouse cardiomyocytes (AMCMs) was validated by assessment of TBC1D15 protein levels using Western blot two weeks following tamoxifen induction (Supporting Information Fig. S3A−S3D). Baseline phenotype of *Tbc1d15*CKO or *Tbc1d15*CKI mice remained unaltered in the absence of stress, consistent with our earlier study[34]. The Kaplan−Meier survival curve saw an approximate 50% mortality in response to DOX challenge in *Tbc1d15* wild type (*Tbc1d15*WT) mice while such response was reduced to only 10% in *Tbc1d15*CKO mice (Fig. 2B). Echocardiographic evaluation, as shown in Fig. 2C−G, revealed that DOX administration overtly increased left ventricular end-systolic diameter (LVESD) and left ventricular end-systolic volume (LVESV), and decreased systolic function as evidenced by lower left ventricular fractional shortening (LVFS) and left ventricular ejection fraction (LVEF) in *Tbc1d15*WT mice, the effects of which were abolished in *Tbc1d15*CKO mice with little effect by *Tbc1d15* ablation itself. Neither DOX challenge nor *Tbc1d15* ablation exerted notable effects on other echocardiographic indices including heart rate, left ventricular end-diastolic diameter (LVEDD), left ventricular end-diastolic volume (LVEDV), interventricular septum thickness (IVS) and left ventricular posterior wall thickness (LVPW) (Fig. 2H−L). In line with left ventricular wall thickness (IVS and LVPW), heart weight to tibial length was unaltered by DOX challenge or *Tbc1d15* deletion (Fig. 2M). Wheat germ agglutinin staining also revealed little change in cardiomyocyte size as evidenced by cardiomyocyte cross-sectional area in *Tbc1d15*WT or *Tbc1d15*CKO mice within 7 days following DOX challenge ($P > 0.05$). *Tbc1d15* deletion alone exhibited little effect on cardiomyocyte size (Fig. 2N and O). For cardiac remodeling, Masson trichrome staining revealed that DOX evoked pronounced interstitial fibrosis, the effect of which was attenuated by *Tbc1d15* deletion with little effect by *Tbc1d15* ablation itself (Fig. 2P and Q).

Gain-of-function examination using *Tbc1d15*CKI mice showed that overexpression of *Tbc1d15* significantly accentuated DOX-induced mortality (Fig. S4B), cardiac geometry (expansion in end-systolic ventricular parameters), and cardiac dysfunction (FS and EF) without affecting heart rate, end-diastolic ventricular parameters and left ventricular wall thickness (Fig. S4C−S4L). *Tbc1d15* overexpression alone exerted little response on these echocardiographic indices. *Tbc1d15* overexpression failed to exert notable effect on heart weight to tibial length ratio and cardiomyocyte size in the absence or presence of DOX (Fig. S4M−S4O). Data from masson staining revealed that DOX-induced interstitial fibrosis was accentuated by *Tbc1d15*
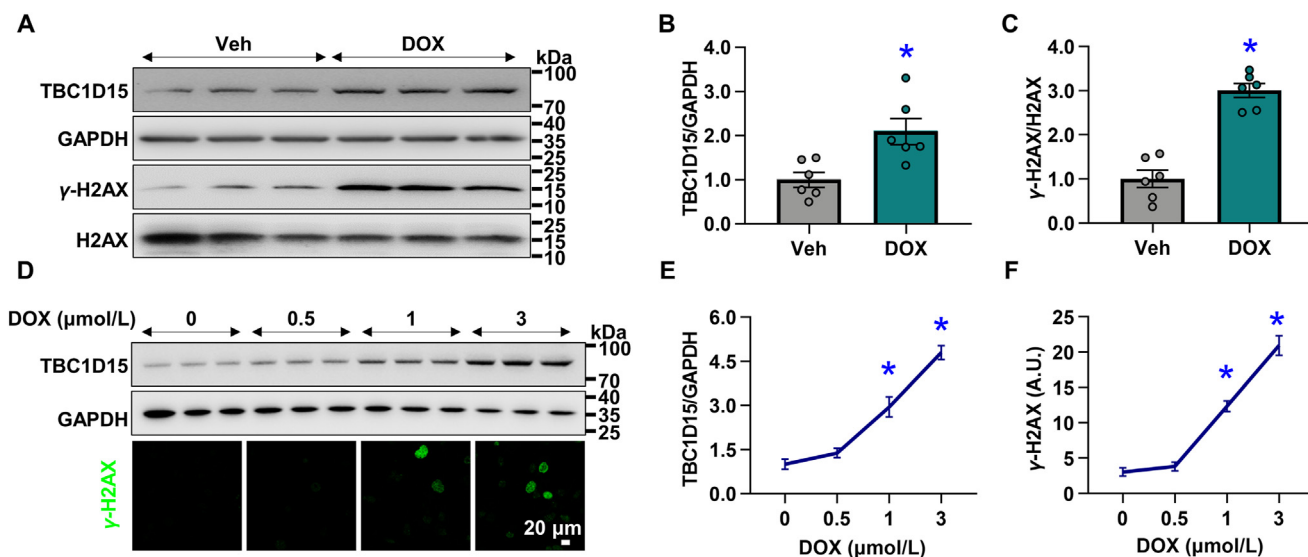
Figure 1 Effect of doxorubicin challenge on TBC1D15 levels in cardiac tissues and cardiomyocytes. (A)−(C) Levels of TBC1D15 and γ-H2A.X/H2A.X ratio in heart tissues from mice following a 7-day doxorubicin (DOX) challenge (12.5 mg/kg, single dose, i.p.) ($n = 6$ mice). (D, E) Protein levels of TBC1D15 in neonatal mouse cardiomyocytes (NMCMs) challenged with indicated concentrations of DOX (0, 0.5, 1, 3 μmol/L) for 24 h ($n = 6$ samples). (F) DNA damage assessed by immunofluorescence of γ-H2A.X staining (Scale bar = 20 μm) ($n = 16, 16, 19,$ and 19 fields). Mean ± SEM, Student's t-test for A−C, one-way ANOVA followed by the Tukey *post hoc* test for D−F, *$P < 0.05$ *vs.* heart tissues from mice or NMCMs treated with vehicle.

overexpression with little effect from *Tbc1d15* overexpression itself (Fig. S4P and S4Q).

3.3. Effect of TBC1D15 on DOX-induced cardiomyocyte apoptosis

To further assess whether TBC1D15 affected apoptosis with DOX exposure, terminal deoxynucleotidyl transferase-mediated dUTP nick end labeling (TUNEL) staining was evaluated. TUNEL positive cells were overtly increased in DOX-challenged mouse hearts. In contrast, fewer TUNEL-positive cells were noted in *Tbc1d15*[CKO] mice in the face of DOX exposure. Cardiac *Tbc1d15* knockout did not affect TUNEL apoptosis in the absence of DOX (Fig. 3A and B). Similarly, levels of pro-apoptotic markers (Bax, cleaved caspase 3, and cleaved caspase 9) were significantly increased while the anti-apoptotic marker Bcl-2 was downregulated in DOX-challenged mouse hearts. Although deletion of *Tbc1d15* itself did not affect apoptosis in the absence of DOX challenge, cardiac knockout of *Tbc1d15* overtly attenuated DOX-induced changes in these apoptosis protein markers (Fig. 3C−G). Serum levels of lactate dehydrogenase (LDH), creatine kinase-MB (CKMB) and cardiac troponin-T (cTnT), indicators of myocardial injury, were significantly elevated in mice challenged with DOX, the effect of which was abrogated by cardiac knockout of *Tbc1d15*. *Tbc1d15* deficiency alone did not exhibit any changes in LDH, CKMB and cTnT levels (Fig. 3H−J). These findings suggest that deletion of *Tbc1d15* is capable of alleviating DOX-induced myocardial injury. Data from gain-of-function study revealed that DOX-induced pronounced cardiomyocyte apoptosis (TUNEL positive cells, Bax, cleaved caspase 3, and cleaved caspase 9, Bcl2) and myocardial injury (LDH, CKMB and cTnT) were accentuated by *Tbc1d15* overexpression with little effect by *Tbc1d15* overexpression itself (Supporting Information Fig. S5A−S5J). Given that earlier findings from our lab and others revealed a role of TBC1D15 in autophagy regulation[35,51,52], autophagy was also monitored. Our data revealed

that DOX evoked significant rises in autophagic protein markers (p62, LC3II, Atg5, Atg7), the effect of which was unaffected by *Tbc1d15* deletion (Fig. S6A−S6E). Likewise, *Tbc1d15* overexpression exerted little effect on DOX-induced rises in both levels of autophagic markers (p62, LC3II, Atg5, Atg7) and number of autophagosomes (Fig. S6F−S6L). These findings suggested a likely role for apoptosis but not autophagy in TBC1D15-evoked regulation on DOX-induced cardiac toxicity.

3.4. Effect of TBC1D15 on DOX-induced mitochondrial anomalies and DNA damage/ATM/p53 cascade

To evaluate the effect of TBC1D15 on DOX-induced mitochondrial anomalies, transmission electron microscopy was applied to monitor morphological changes of mitochondria in heart slice. As shown in Fig. 4A−C, DOX challenge evoked overt rises in mitochondrial damage characterized by swelling, deformation, cristae fracture and rupture, and elevation of mitochondrial circularity index, all of which were significantly attenuated by *Tbc1d15* deletion. Cardiac *Tbc1d15* knockout alone did not exert any notable change on mitochondrial ultrastructure. Meanwhile, cardiomyocytes were challenged with DOX in the absence or presence of adenoviral transfection of *Tbc1d15* or *Tbc1d15* knockdown. Since AMCMs were mostly dead when challenged with high levels of DOX (>1 μmol/L), DOX was administrated at the concentration of 1 μmol/L for 24 h. Western blot was employed to optimize MOI condition of adenoviruses overexpressing *Tbc1d15* and shRNA sequence of *Tbc1d15* (Supporting Information Fig. S7A and S7B). Mitochondrial membrane potential (MMP) was assessed using tetramethylrhodamine methyl ester (TMRM) staining. Data revealed a significant decrease of TMRM intensity in cardiomyocytes following DOX exposure for 24 h. Interestingly, DOX-induced decline in TMRM was significantly accentuated by *Tbc1d15* overexpression while the DOX response was overtly alleviated by *Tbc1d15* knockdown. Neither
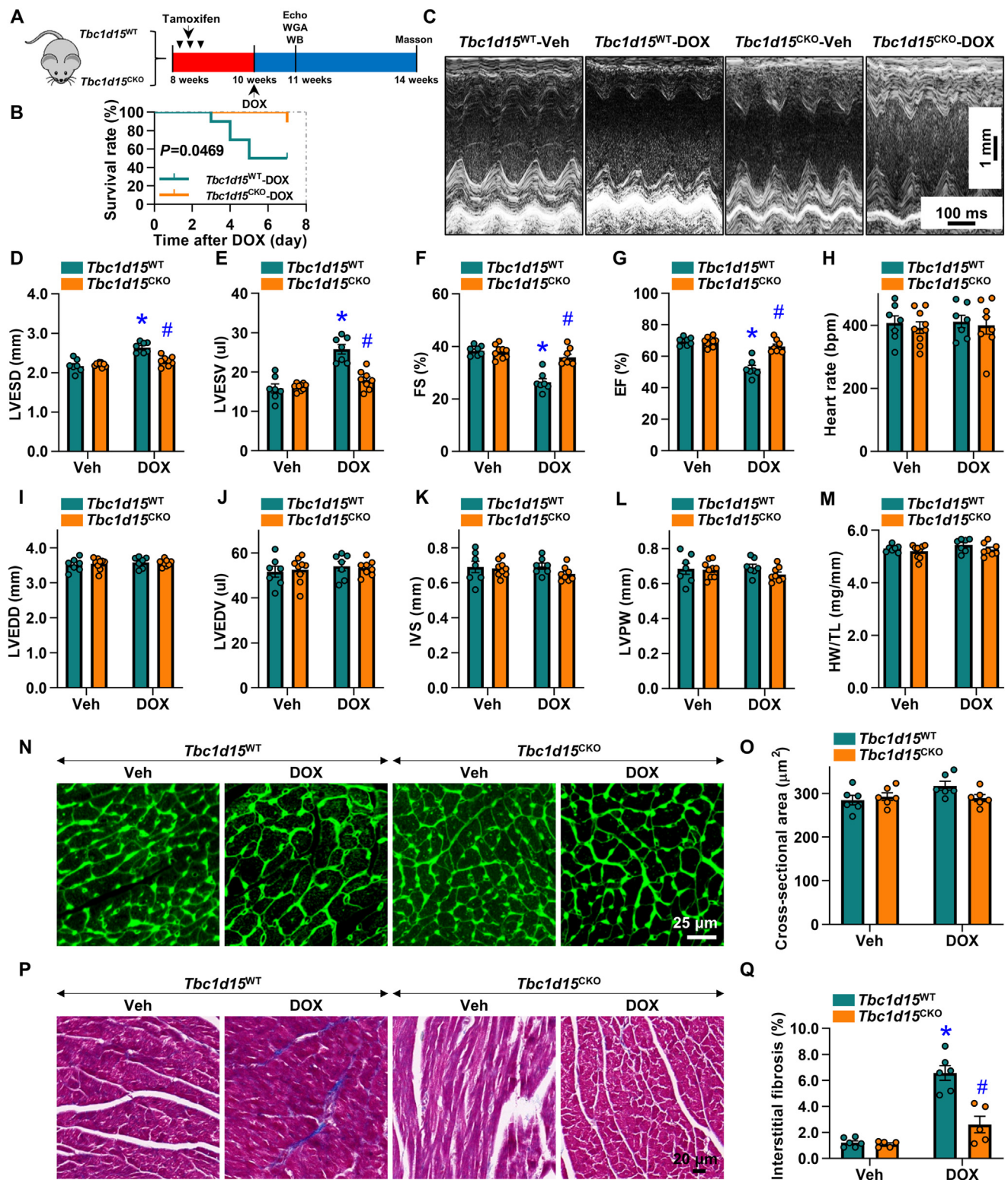
Figure 2 Effect of TBC1D15 on DOX-induced changes in myocardial function and morphology. (A) Loss-of-function study protocol; (B) Kaplan−Meier survival curves of *Tbc1d15*^{WT} and *Tbc1d15*^{CKO} mice challenged with or without DOX (*n* = 10 and 9 mice); (C) Representative echocardiographic images; (D) Left ventricular end-systolic diameter (LVESD); (E) Left ventricular end-systolic volume (LVESV); (F) Fractional shortening (FS); (G) Ejection fraction (EF); (H) Heart rate; (I) Left ventricular end-diastolic diameter (LVEDD); (J) Left ventricular end-diastolic volume (LVEDV); (K) Interventricular septum thickness (IVS); (L) Left ventricular posterior wall thickness (LVPW) (*n* = 7, 9, 7, and 8 mice); (M) Heart weight to tibial length (HW/TL) (*n* = 7, 9, 7, and 8 mice); (N, O) Representative and pooled cross-sectional area (Scale bar = 25 μm) of cardiomyocytes in heart tissues from *Tbc1d15*^{WT} and *Tbc1d15*^{CKO} mice challenged with or without DOX (*n* = 6 mice); and (P, Q) Interstitial
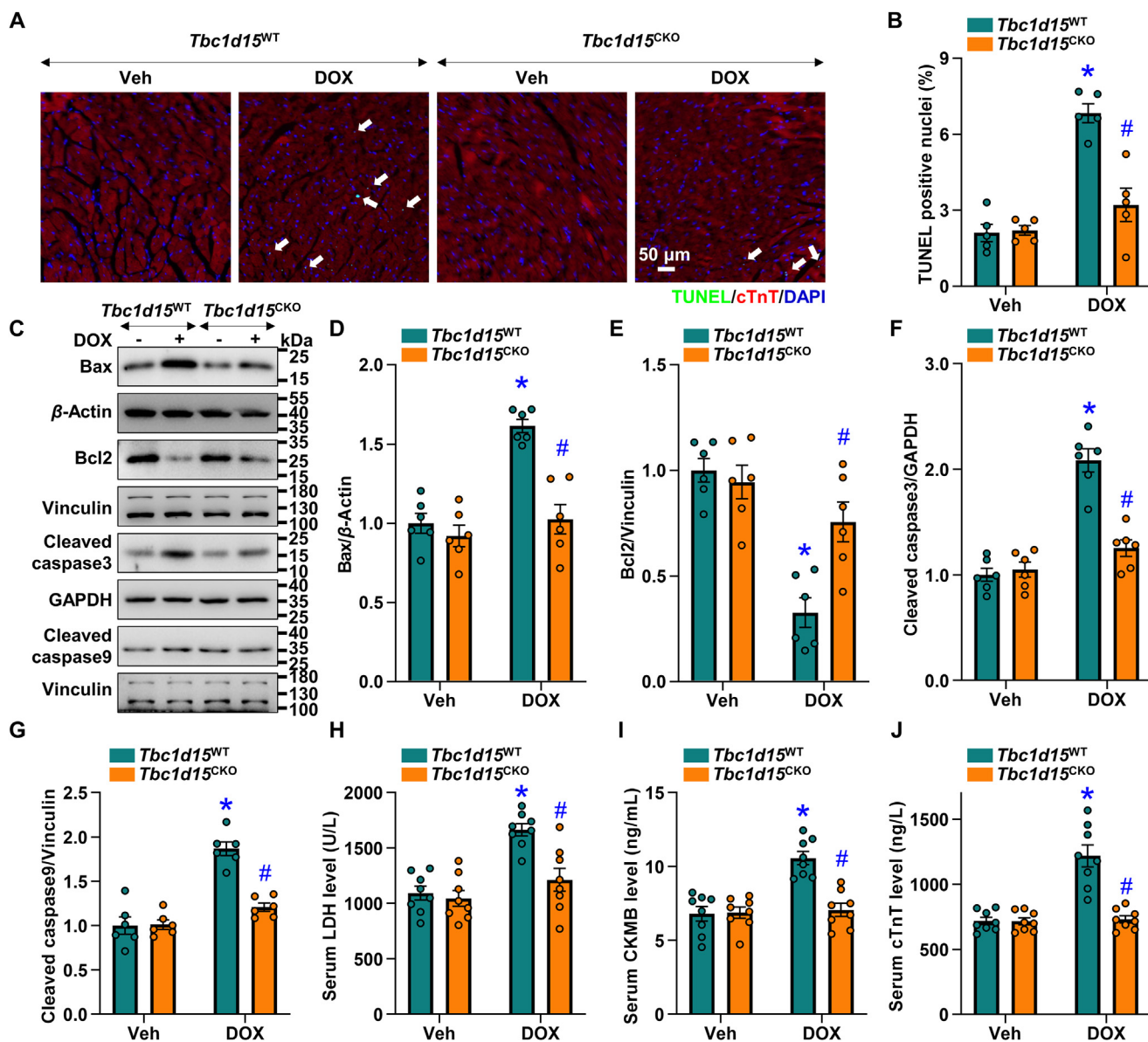
Figure 3 Effect of TBC1D15 on DOX-induced cardiomyocyte apoptosis. (A, B) Representative and pooled cardiomyocyte apoptosis assessed using terminal deoxynucleotidyl transferase-mediated dUTP nick end labeling (TUNEL)/DAPI/cTnT staining (Scale bar = 50 μm) in $Tbc1d15^{WT}$ and $Tbc1d15^{CKO}$ mice challenged with or without DOX (n = 5 mice). The white arrowheads indicate the TUNEL positive nuclei; (C)−(G) Cardiomyocyte apoptotic markers (Bax, Bcl2, cleaved caspase3 and cleaved caspase9, normalized to respective loading controls) (n = 6 mice); and (H)−(J) Serum markers of myocardial injury (LDH, CKMB and cTnT) (n = 8 mice). Mean ± SEM, two-way ANOVA followed by the Tukey *post hoc* test, *P < 0.05 *vs. Tbc1d15*^{WT}-Veh group, #P < 0.05 *vs. Tbc1d15*^{WT}-DOX group.

maneuver alone exerted any effect on TMRM intensity (Fig. 4D and E). Furthermore, oxidative stress and redox status were evaluated using mitoSOX, reactive oxygen species (ROS) staining and GSH/GSSG. Our results show that 24 h DOX challenge induced dramatical rises in mitoSOX and ROS intensity along with a significant drop in GSH/GSSG ratio, the effects of which were significantly exaggerated and ameliorated by *Tbc1d15* overexpression and knockdown, respectively. Neither *Tbc1d15* overexpression nor knockdown alone exerted any effect on these indices for oxidative stress and redox status (Fig. 4F−J).

Mitochondrial dysfunction and oxidative stress are closely associated with DNA damage and DNA damage response (DDR)[53]. ATM and p53 are phosphorylated at Ser1981 and Ser15, respectively, in response to DNA double-strand breaks (DSBs)[53]. To evaluate possible involvement of TBC1D15 in DDR, ATM/p53 cascade was assessed. Western blot showed that ATM(Ser1981) and p53(Ser15) levels were both increased following DOX challenge. Cardiac *Tbc1d15* knockout significantly attenuated ATM(Ser1981) and p53(Ser15) levels (Fig. 4K−M). Further detection of DNA damage using γH2A.X staining displayed a

fibrosis (Scale bar = 20 μm) in heart tissues from $Tbc1d15^{WT}$ and $Tbc1d15^{CKO}$ mice challenged with or without DOX (n = 6, 5, 6, and 5 mice). Mean ± SEM, Gehan−Breslow−Wilcoxon test for Kaplan−Meier survival curves, two-way ANOVA followed by the Tukey *post hoc* test for others, *P < 0.05 *vs. Tbc1d15*^{WT}-Veh group, #P < 0.05 *vs. Tbc1d15*^{WT}-DOX group.
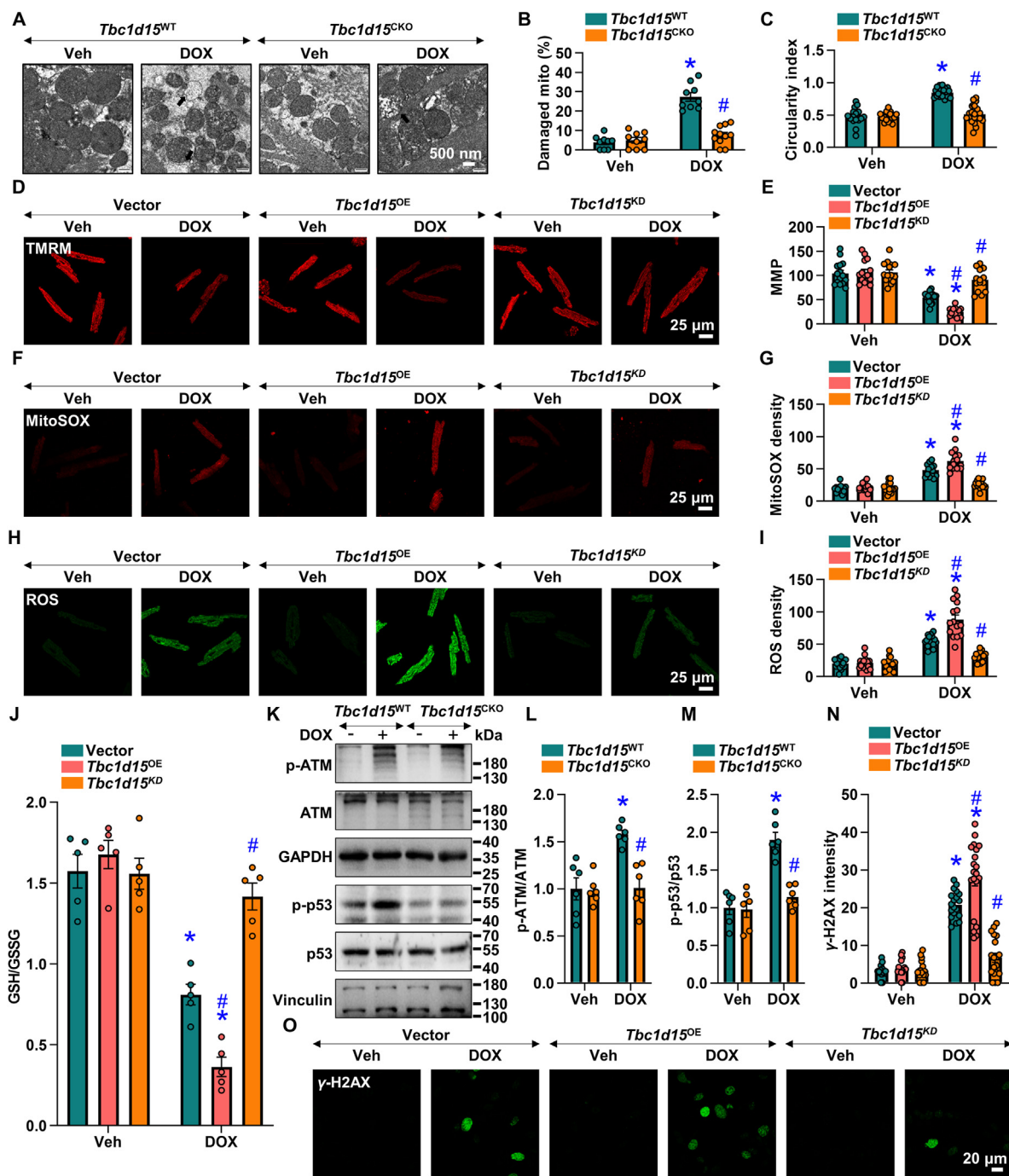
Figure 4 Effect of TBC1D15 on DOX-induced mitochondrial anomalies and DNA damage/ATM/p53 cascade. (A)−(C) Representative and pooled transmission electron microscopy ultrastructure showing damaged mitochondria ($n = 9, 9, 9$, and 11 fields) and circularity index ($n = 18$, 18, 18, and 22 fields) (Scale bar = 500 nm). The black arrow indicates the damaged mitochondrion; (D, E) Representative and pooled mito-chondrial membrane potential (MMP) assessed by tetramethylrhodamine methyl ester (TMRM) staining (Scale bar = 25 μm) in adult mouse cardiomyocytes (AMCMs) transfected with vector, *Tbc1d15*-overexpressed (*Tbc1d15*^OE) or *Tbc1d15*-knockdown (*Tbc1d15*^KD) adenovirus in the presence or absence of DOX (1 μmol/L for 24 h) ($n = 15$ fields); (F)−(I) Oxidative stress by mitoSOX ($n = 15, 15, 14, 15, 15$ and 15 fields) and reactive oxygen species (ROS) staining ($n = 15$ fields) (Scale bar = 25 μm); (J) GSH to GSSG ($n = 5$ samples); (K)−(M) Levels of ATM and p53 (normalized to loading control) in *Tbc1d15*^WT and *Tbc1d15*^CKO mice following DOX challenge ($n = 6$ mice); and (N, O) Representative and pooled DNA damage assessed using γ-H2A.X staining of NMCMs transfected with vector, *Tbc1d15*^OE or *Tbc1d15*^KD adenovirus in the presence or absence of DOX (3 μmol/L for 24 h) (Scale bar = 20 μm) ($n = 16, 16, 16, 19, 20$, and 19 fields). Mean ± SEM, two-way ANOVA followed by the Tukey *post hoc* test, *$P < 0.05$ *vs.* *Tbc1d15*^WT-Veh group or AdVector-Veh group, #$P < 0.05$ *vs.* *Tbc1d15*^WT-DOX group or AdVector-DOX group.

dramatical rise in γH2A.X intensity in cardiomyocytes following DOX exposure for 24 h. Interestingly, 24-h DOX-induced rise in γH2A.X intensity was significantly aggravated by *Tbc1d15* overexpression while such DOX response was overtly attenuated by *Tbc1d15* knockdown. Neither treatment alone exerted little effect on γH2A.X intensity (Fig. 4N and O). Etoposide and camptothecin were also used to evaluate the effect of TBC1D15 on DNA damage. Western blot results showed that ratio of γH2A.X-to-H2A.X was overtly increased in NMCMs challenged with etoposide or camptothecin, the effect of which was alleviated by *Tbc1d15* knockdown (Fig. S7C and S7D). These findings have depicted a likely role for TBC1D15 in DOX-evoked DNA damage, activation of ATM/p53 cascade and mitochondrial anomalies.

3.5. Effect of TBC1D15 on DOX-induced cytosolic DNA-dependent protein kinase catalytic subunit (DNA-PKcs) accumulation

Previous studies have noted increased levels and activity of DNA-PKcs in DOX-induced DNA damage[19]. Nuclear DNA-PKcs is critical for DNA damage repair. Levels of DNA-PKcs were assessed. NMCMs were challenged with DOX for 24 h at 0, 0.5, 1, and 3 μmol/L. Immunofluorescence stained with DNA-PKcs and DAPI showed accumulated cytosolic DNA-PKcs dots in cardiomyocytes with 1 μmol/L DOX challenge, with a more prominent response at 3 μmol/L DOX (Fig. 5A and B). Three-dimensional imaging confirmed cytosolic DNA-PKcs accumulation (Fig. 5C). Interestingly, cytosolic DNA-PKcs accumulation was aggravated by *Tbc1d15* overexpression while such response was attenuated by *Tbc1d15* knockdown with DOX (3 μmol/L) challenge for 24 h. Neither *Tbc1d15* maneuver alone exerted any discernible effect on cytosolic DNA-PKcs accumulation (Fig. 5D and E). Unfortunately, DNA-PKcs fluorescence was undetectable in nuclei of NMCMs despite the usage of high concentration of primary antibody. Nevertheless, further detection from fractional components (nucleus and cytosol) showed that nuclear DNA-PKcs level was increased at 0.5 μmol/L prior to a decline at > 1 μmol/L. However, cytosolic DNA-PKcs level was increased at 1 and 3 μmol/L DOX (Fig. 5F−H). *Tbc1d15* overexpression significantly aggravated cytosolic DNA-PKcs elevation while *Tbc1d15* knockdown attenuated DNA-PKcs distribution anomalies. Neither overexpression nor knockdown of *Tbc1d15* exerted any effect on DNA-PKcs distribution (Fig. 5I−K). Cytosolic accumulation of DNA-PKcs dots was also evident in mouse myocardium 7 days after DOX challenge using immunofluorescence with DNA-PKcs, DAPI and WGA, the effects of which were attenuated by cardiac knockout of *Tbc1d15* in mice (Fig. 5L and M). In contrast, *Tbc1d15* overexpression *in vivo* significantly exacerbated cytosolic accumulation of DNA-PKcs dots (Fig. 5N and O). Fixed heart sections with or without DOX challenge were incubated with a secondary antibody in the absence of a DNA-PKcs primary antibody to rule out possible effect of DOX autofluorescence (Red) (Supporting Information Fig. S7E), as suggested in a previous report[14].

TBC1D15 functions as a GTPase-activating protein for RAB7 or RAB11[31]. To this end, protein levels of RAB7 and RAB11 were monitored in myocardium from DOX-challenged mice. Data showed that DOX downregulated levels of RAB7 and RAB11 compared with vehicle (Supporting Information Fig. S8A and S8B). In line with *in vivo* results, DOX also downregulated levels of RAB7 and RAB11 *in vitro*. However, neither overexpression nor knockdown of *Tbc1d15* exerted any discernible

effects on DOX-induced changes in RAB7 and RAB11 (Fig. S8C and S8D). Moreover, γH2A.X staining showed little effect of *Rab7* or *Rab11* knockdown through respective RNA interference on DOX-induced DNA damage (Fig. S8E and S8F). Western blot was applied to screen various siRNA sequences of *Rab7* (Fig. S8G) or *Rab11* (Fig. S8H). These results do not favor a major role for RAB7 or RAB11 in TBC1D15-mediated response against DOX cardiotoxicity.

3.6. Interaction between TBC1D15 and DNA-PKcs

Next, protein candidates possibly interacting with TBC1D15 were evaluated using unbiased proteomic analysis in *Tbc1d15*-overexpressed cardiomyocytes. Tandem mass spectrometry analysis following affinity purification identified 424 proteins putatively bound to TBC1D15 in *Tbc1d15*-transfected cardiomyocytes but not in cells without *Tbc1d15* transfection. Focusing on protein candidates associated with DNA and apoptosis (biological process), 76 proteins in particularly the top 5 proteins were enriched and displayed in Table S4. Among these candidates, DNA-PKcs, a member of the phosphatidylinositol 3-kinase-related family of protein kinases, ranked atop as one of 5 candidates to bind TBC1D15 in cardiomyocytes (Fig. 6A). Further immunoprecipitation analysis revealed a strong interaction between TBC1D15 and DNA-PKcs in cardiomyocytes (Fig. 6B). TBC1D15 contains four distinct domains including RAB7 binding, Fis1 binding, RAB-GTPase activating protein (GAP) domains, and an unidentified domain (aa 564−671). Prediction of TBC1D15 sites bound with DNA-PKcs using Prism software showed that binding sites were localized within the Fis1 binding, RAB-GAP or 564−671 domains, with the unidentified TBC1D15 domain (aa 564−671) possessing the highest probability (Fig. 6C). To this end, TBC1D15 mutants targeting these domains exhibited in Fig. 6D were constructed. Immunoprecipitation analysis revealed that segment of TBC1D15 (aa 594−624) mediated TBC1D15/DNA-PKcs interaction rather than segments of TBC1D15 (aa 280−320, the Fis1 binding domain) and TBC1D15 (aa 476−506, the RAB-GAP domain) (Fig. 6E).

3.7. Effect of TBC1D15/DNA-PKcs interaction on DNA-PKcs distribution and DNA damage

To evaluate effects of TBC1D15/DNA-PKcs interaction on DOX-induced DNA-PKcs distribution, DNA damage and cardiomyocyte apoptosis, adenoviruses containing TBC1D15 (total length, TL) and TBC1D15 (Δ594−624) was constructed and delivered into cardiomyocytes challenged with or without DOX. Immunofluorescence analysis also showed increased cytosolic DNA-PKcs dots and γH2A.X intensity in cardiomyocytes following DOX challenge. *Tbc1d15* overexpression significantly aggravated DNA-PKcs dots accumulation and γH2A.X intensity in DOX-challenged myocardium while deletion of TBC1D15 (aa 594−624) failed to duplicate the response of TBC1D15 (TL). Neither TBC1D15 (TL) or TBC1D15 (Δ594−624) exerted any effect on DNA-PKcs dots accumulation and γH2A.X intensity (Fig. 6F and G). For apoptosis analysis, AMCMs were isolated from tamoxifen-induced *Tbc1d15*[CKO] mice and were then transfected with adenoviruses encoding TBC1D15 (TL) and TBC1D15 (Δ594−624). TUNEL assay showed that 24-h DOX exposure induced pronounced TUNEL apoptosis. *Tbc1d15* deletion overtly attenuated while TBC1D15 (TL) re-expression significantly aggravated DOX-induced TUNEL apoptosis, the effect of which was not
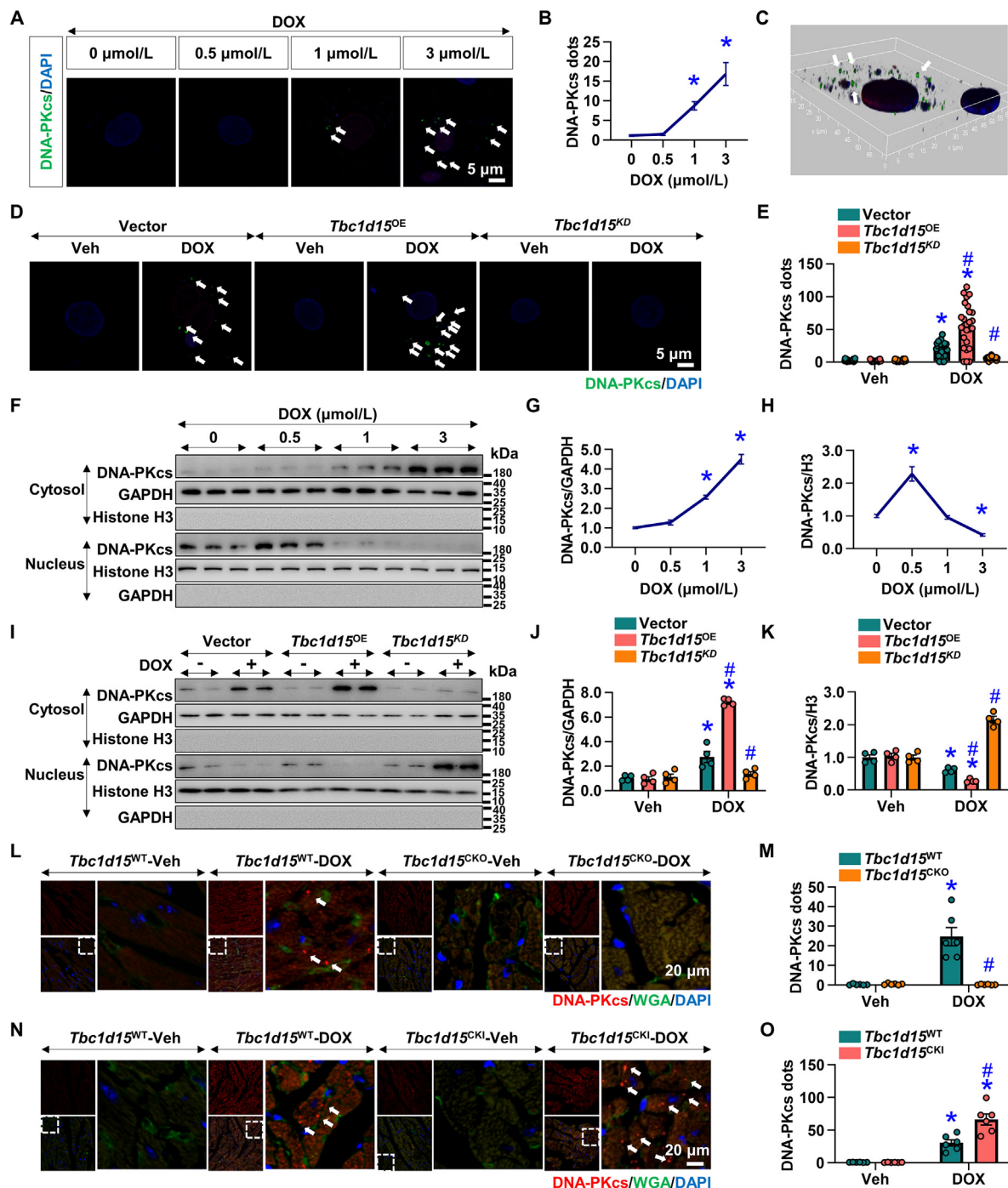
Figure 5 Effect of TBC1D15 on DOX-induced cytosolic DNA-PKcs accumulation. (A)−(C) DNA-PKcs fluorescence intensity (Scale bar = 5 μm) in NMCMs challenged with indicated doses of DOX (n = 19, 19, 19, and 21 fields). The three-dimensional imaging of cytosolic DNA-PKcs accumulation was exhibited in (C); (D, E) DNA-PKcs/DAPI staining (Scale bar = 5 μm) of NMCMs transfected with vector, $Tbc1d15^{OE}$ or $Tbc1d15^{KD}$ adenovirus in the presence or absence of DOX (n = 20, 20, 20, 26, 26, and 20 fields); (F)−(H) Fractional components (nucleus and cytosol) detection of TBC1D15 in NMCMs challenged with indicated concentrations of DOX (n = 6 samples); (I)−(K) Fractional components (nucleus and cytosol) detection of TBC1D15 in NMCMs transfected with aforementioned adenoviruses in the absence or presence of DOX (n = 4 samples); and (L)−(O) Cytosolic DNA-PKcs assessed by DNA-PKcs/wheat germ agglutinin (WGA)/DAPI staining (Scale bar = 20 μm) in $Tbc1d15^{WT}$, $Tbc1d15^{CKO}$ mice or $Tbc1d15^{CKI}$ mice following DOX challenge (n = 6 mice). The white arrows in (A), (C), (D), (L) and (N) indicate the DNA-PKcs positive dots. Mean ± SEM, one-way ANOVA followed by the Tukey *post hoc* test for A−B and F−H, two-way ANOVA followed by the Tukey *post hoc* test for others, *P < 0.05 *vs.* NMCMs treated with vehicle, or AdVector-Veh group, or $Tbc1d15^{WT}$-Veh group, #P < 0.05 *vs.* AdVector-DOX group or $Tbc1d15^{WT}$-DOX group.
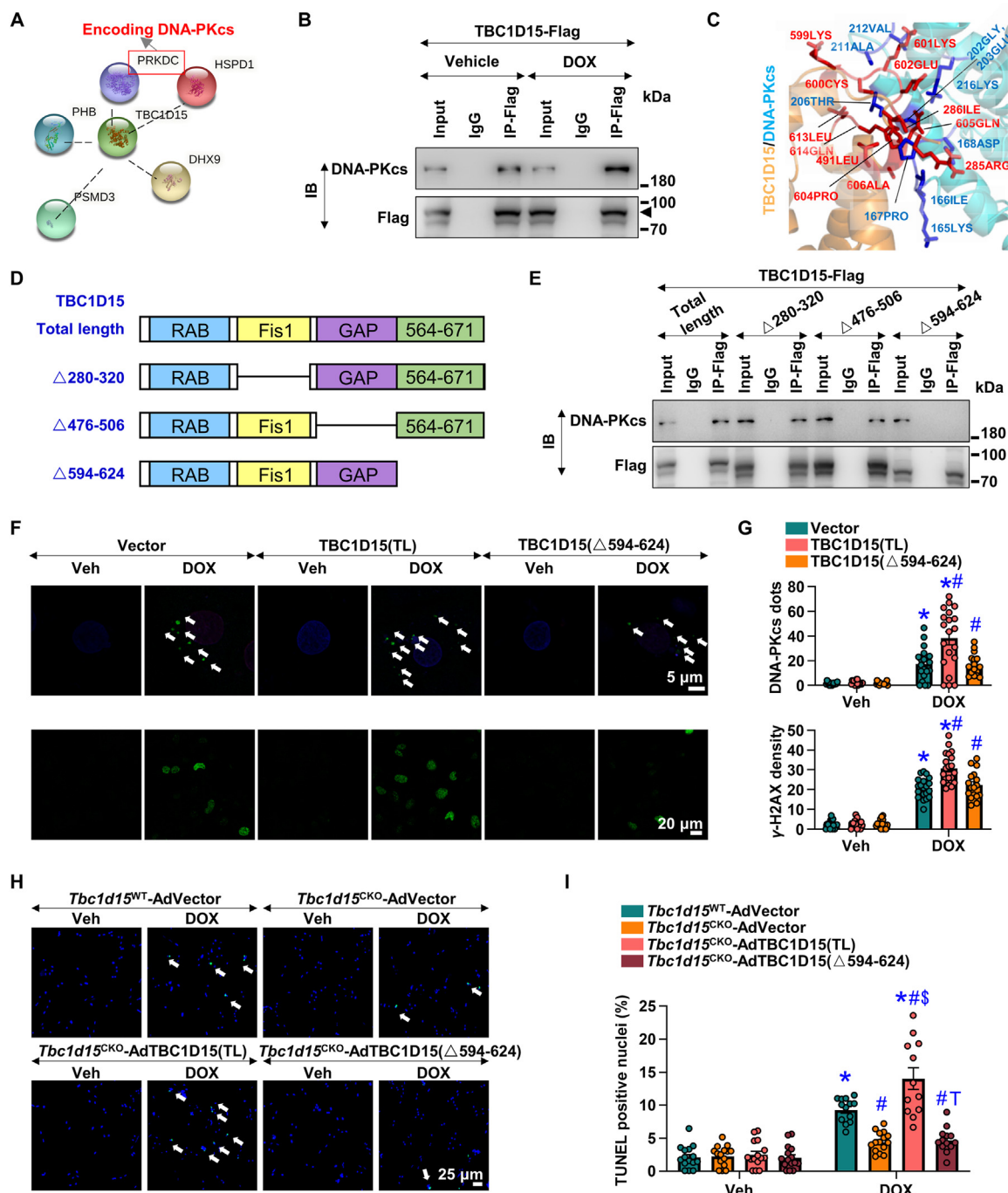
Figure 6 TBC1D15/DNA-PKcs interaction and its effect on DNA-PKcs distribution and DNA damage. (A) Liquid chromatography-tandem mass spectrometry analysis showing top 5 candidates binding with TBC1D15; (B) Immunoprecipitation analysis; (C) Prediction of TBC1D15 sites binding with DNA-PKcs; (D) Graph illustrating construction of TBC1D15 (total length, TL) and mutants ($\Delta 280-320$, $\Delta 476-506$, $\Delta 594-624$); (E) Immunoprecipitation analysis; (F, G) Fluorescence analysis of DNA-PKcs (Scale bar = 5 μm) and γ-H2A.X staining (Scale bar = 20 μm) in NMCMs transfected with vector, TBC1D15 (TL)- or TBC1D15 ($\Delta 594-624$)-overexpressed adenovirus after DOX challenge. The white arrows indicate the DNA-PKcs positive dots. n = 16, 16, 17, 20, 20, and 17 fields for DNA-PKcs/DAPI staining and n = 16, 17, 16, 20, 20, and 17 fields for γ-H2A.X staining; and (H, I) Apoptosis by TUNEL/DAPI staining (Scale bar = 25 μm) of AMCMs isolated from $Tbc1d15^{WT}$ and $Tbc1d15^{CKO}$ mice in the absence or presence of DOX and transfected with vector, TBC1D15 (TL)- or TBC1D15 ($\Delta 594-624$)-overexpressed adenovirus (n = 15, 15, 15, 15, 13, 15, 12, and 13 fields). The white arrows indicate the TUNEL positive nuclei. Mean ± SEM, two-way ANOVA followed by the Tukey *post hoc* test, *P < 0.05 *vs.* AdVector-Veh group or $Tbc1d15^{WT}$-AdVector-Veh group, #P < 0.05 *vs.* AdVector-DOX group or $Tbc1d15^{WT}$-AdVector-DOX group, P < 0.05 *vs.* $Tbc1d15^{CKO}$-AdVector-DOX group, †P < 0.05 *vs.* $Tbc1d15^{CKO}$-AdTBC1D15 (TL)-DOX group.

exacerbated by TBC1D15 mutant (Δ594−624). *Tbc1d15* deficiency, TBC1D15 (TL) re-expression or TBC1D15 (Δ594−624) failed to exert any effect on the number of TUNEL-positive cells in the absence of DOX (Fig. 6H and I).

3.8. Effect of TBC1D15/DNA-PKcs/ATM cascade on DOX-induced cardiomyocyte contractile anomalies

To further evaluate the effect of TBC1D15/DNA-PKcs/ATM cascade on DOX-induced cardiotoxicity, AMCMs from tamoxifen-induced *Tbc1d15*[CKO] mice were isolated and treated with NU7441 (DNA-PKcs inhibitor) or floxuridine (ATM activator) for 24 h in the presence or absence of DOX. Analysis of cardiomyocyte contractile property showed that 24 h DOX exposure suppressed peak shortening, maximal velocity of shortening/relengthening ($\pm dL/dt$) as well as prolonged time-to-90% relengthening (TR_{90}) without affecting resting cell length and time-to-peak shortening (TPS). *Tbc1d15* knockout attenuated DOX-induced cardiomyocyte mechanical abnormalities, the effect of which was cancelled off by either inhibition of DNA-PKcs or activation of ATM. *Tbc1d15* knockout, NU7441 or floxuridine treatment failed to alter cardiomyocyte mechanical indices in the absence of DOX challenge (Supporting Information Fig. S9A−S9F).

3.9. Impact of TBC1D15/DNA-PKcs/ATM cascade on DOX-induced cardiomyocyte apoptosis, mitochondrial anomalies, DNA damage and cytosolic DNA-PKcs accumulation

NMCMs from tamoxifen-induced *Tbc1d15*[CKO] mice were isolated and were incubated with NU7441 (DNA-PKcs inhibitor) or floxuridine (ATM activator). TUNEL assay showed that *Tbc1d15* knockout attenuated DOX-induced cardiomyocyte apoptosis, the effect of which was nullified by either inhibition of DNA-PKcs or activation of ATM (Supporting Information Fig. S10A and S10B). TMRM and mitoSOX staining indicated that *Tbc1d15* knockout alleviated DOX-induced collapse of mitochondrial membrane potential and rises of mitochondrial oxidative stress, the effects of which were mitigated by inhibition of DNA-PKcs or activation of ATM (Supporting Information Fig. S11A−S11D). Immunofluorescence staining also noted that *Tbc1d15* knockout annihilated DOX-induced rise in γH2A.X intensity and cytosolic DNA-PKcs accumulation, the effects of which were removed by inhibition of DNA-PKcs or activation of ATM (Supporting Information Fig. S12A−S12D). *Tbc1d15* knockout, NU7441 or floxuridine failed to notably affect cardiomyocyte apoptosis, mitochondrial membrane integrity, DNA damage and cytosolic DNA-PKcs accumulation in the absence of DOX challenge.

4. Discussion

The salient findings from our current study revealed a detrimental role for TBC1D15 in doxorubicin (DOX)-induced cardiotoxicity. DOX overtly upregulated TBC1D15 levels, in line with elevated TBC1D15 levels in human dilated cardiomyopathy (DCM) heart samples. Our results revealed that DOX challenge evoked cardiac remodeling and contractile dysfunction, the effects of which were ameliorated and accentuated, respectively, by deletion and overexpression of *Tbc1d15*. Furthermore, overexpression of *Tbc1d15* aggravated while depletion of *Tbc1d15* attenuated DOX-induced DNA-damage, mitochondrial anomalies and apoptosis. Mechanistic scrutiny noted that TBC1D15 directly bound and interacted

with DNA-PKcs, leading to DNA-PKcs retention in the cytosol to diminish its nuclear translocation. As a result, DNA double-strand breaks (DSBs) repair was dampened to exacerbate DOX-induced DNA damage, resulting in activation of ATM/p53 cascade, mitochondrial anomalies and oxidative stress. This is supported by the fact that TBC1D15 mutant (Δ594−624) failed to elicit any aggravating effects elicited by TBC1D15 (WT) on DOX-induced cardiac responses. Conversely, *Tbc1d15* deletion-mediated attenuation of DOX-induced cardiomyocyte abnormalities was cancelled off by inhibition of DNA-PKcs or activation of ATM. These actions of TBC1D15 under DOX challenge, through regulation of DNA-PKcs cytosolic retention, DNA damage and apoptosis, ultimately prompt cardiac remodeling, contractile dysfunction, apoptotic cell death, and animal mortality, as seen in *Tbc1d15*[CKI] mice. Our work represents the first study to delineate a vital role for TBC1D15 in the pathogenesis of DOX-induced cardiotoxicity through mechanisms involving DNA-PKcs distribution, DNA damage/DSBs repair, mitochondrial function and cell death.

DOX exposure evokes cardiotoxicity manifested by unfavorable structural and functional changes in the heart including cardiac hypertrophy, compromised cardiac contractility, ventricular dilation in concert with cell death, oxidative stress[10,11] and autophagy derangement[14]. This is supported by our current findings of enlarged left ventricular end-systolic diameter, reduced fractional shortening, ejection fraction, peak shortening, maximal velocity of shortening and prolonged time-to-90% relengthening following DOX challenge. Mortality usually occurs as a result of severe cardiac dysfunction. However, cardiac hypertrophy was absent in our experimental setting with little changes in left ventricular wall thickness and cardiomyocyte cross-sectional area. The discrepancy may be related to difference in dosage or duration of DOX. Four weeks following DOX challenge, cardiac remodeling is evident with pronounced interstitial fibrosis. We further revealed mitochondrial ultrastructural anomalies (swelling, deformation, and cristae fracture), oxidative stress and loss of mitochondrial membrane potential (TMRM, mitoSOX, ROS), unchecked autophagy and apoptosis following DOX challenge. Deficiency in *Tbc1d15* dramatically attenuated whereas *Tbc1d15* overexpression accentuated DOX-induced myocardial dysfunction, interstitial fibrosis, apoptosis, mitochondrial structural anomalies, and oxidative stress (but not autophagy). These results convincingly support an obligatory role for TBC1D15 in DOX-induced cardiac dyshomeostasis and cardiotoxicity.

DNA damage is perhaps the most striking sequelae induced by DOX[7,8]. In our hands, DOX elicited pronounced DNA damage as evidenced by accumulation of γH2A.X dots. As a member of the phosphatidylinositol 3-kinase-related family, DNA-PKcs is mainly turned on by DNA damage, aging, radiation, oxidative stress, asthma and type 2 diabetes mellitus[53]. We found elevated DNA-PKcs levels in cells with low level of DOX, albeit DNA-PKcs was gradually downregulated with higher levels of DOX exposure. These findings are consistent with the previous notion for a beneficial role for DNA-PKcs-mediated DNA repair in DOX-induced cardiotoxicity[53]. More evidence revealed a role for ATM activation and p53 phosphorylation in DOX-induced DNA damage in the heart, while inhibition of p53 reversed DOX-induced deleterious effects[19,20,54]. Data from our present study noted that deletion of *Tbc1d15* overtly attenuated γH2A.X dots with little effect on total DNA-PKcs levels. This is further supported by suppression of DOX-induced activation of DNA damage/ATM/p53 signaling cascade with ablation of *Tbc1d15*. Further evidence from etoposide and camptothecin results would support a

universal protective effect of TBC1D15 inhibition against DNA damage. These findings collectively favor a prominent role for TBC1D15 from TBC-domain-containing protein family as a cytosolic regulator for nuclear DNA repair.

TBC1D15 belongs to TBC domain-containing proteins containing a conserved protein motif consisting of approximately 200 amino acids[55]. As a GTPase activating proteins for the small GTPase Rab, TBC domain-containing proteins promote hydrolysis of Rab-GTP to Rab-GDP involved in specific intracellular trafficking processes. To date, at least 40 TBC proteins have been identified with proven roles in many chronic diseases including diabetes mellitus[56], obesity[57], cancer[58], neurological diseases[59], atopic dermatitis[60] and viral infection[61]. TBC1D15 participates in multiple biological processes[35] especially neurological disorders[62]. Previous work from our group demonstrated a role for TBC1D15 in acute myocardial infarction (MI)[35] and myocardial ischemia-reperfusion[34]. Here our current data noted that deletion of *Tbc1d15* effectively preserved cardiac morphology, contractile function, mitochondrial function and cell survival with alleviated DNA damage in the face of DOX, in contrast to its seemingly beneficial role in acute MI[35], I/R[34] and neurological disorders[62]. Such discrepancy, although not fully elucidated, may be associated with distinct levels of the TBC1D15 downstream effectors including RAB7 and RAB11 under various pathological settings. RAB7 and RAB11 were upregulated in acute MI while they were downregulated in DOX-induced cardiotoxicity. RAB7 and RAB11 serve as an obligatory factor for TBC1D15-exerted beneficial effects. Nonetheless, data from our current study did not favor an important role for RAB7 and RAB11 in TBC1D15-mediated myocardial responses in the face of DOX challenge.

DNA-PKcs was originally reported to reside and function in the nucleus. Under physiological settings, DNA-PKcs primarily binds to Ku80[28], which functions as an intrinsic repair machinery to repair damaged DNA by recognizing and interacting with broken segments of DNA. Data from our study report for the first time that TBC1D15 directly binds with DNA-PKcs to promote its DNA-PKcs cytosolic retention in conjunction with lessened nuclear translocation of DNA-PKcs. TBC1D15 mutant (which disengages its interaction with DNA-PKcs) nullified total-length TBC1D15-evoked deleterious effect as evidenced by cytosolic DNA-PKcs dots, γH2A.X dots and apoptotic cells. Inhibition of DNA-PKcs or activation of its downstream signaling effector ATM cancelled off *Tbc1d15* deletion-offered protection against DOX-induced cardiomyocyte contractile anomalies, cardiomyocyte apoptosis, mitochondrial anomalies, DNA damage and cytosolic DNA-PKcs accumulation. More recent evidence has documented innovative non-genomic functions of DNA-PKcs and depicted a complex role for DNA-PKcs in cells[25,27,63−66]. Whether TBC1D15-regulated cytosolic accumulation of DNA-PKcs possesses any non-genomic properties in DOX-induced cardiotoxicity deserved to be further examined. In addition, many proteins, biological processes, and signaling cascades have been implicated in DOX cardiomyopathy[8]. For example, recent studies implicated a vital role of ferroptosis in DOX-induced cardiomyopathy[67,68]. As mitochondrial damage such as mitochondrial DNA stress and mitochondrial oxidative stress triggers ferroptosis, TBC1D15 and DNA-PKcs interaction could participate in DOX-induced ferroptosis regulation. Further study is warranted to elucidate the possible interaction among these signaling cascades in DOX cardiomyopathy.

Experimental limitations: Several limitations exist for our study. First and foremost, although DOX was commonly employed to establish a murine model for DCM[6,14,40,42], our set of DCM patients was not exposed to DOX. A more specific patient set would be needed who have received DOX for some time with development of DCM. Caution should be taken in extrapolation of our clinical data. Next, we only used male mice for animal study (inconsistent with human profile). More studies should be taken to evaluate potential sex discrepancy in TBC1D15-evoked response in DOX-induced cardiomyopathy. Third, although our study favors a cardinal role for DNA damage in TBC1D15-evoked responses, additional contributing factors including transcriptome aberrations[9], mitochondrial iron accumulation[12], inflammation[13] and other regulated cardiomyocyte death pathways[69] (ferroptosis, necroptosis, pyroptosis) have all been documented in DOX cardiotoxicity, and cannot be ruled out at this time. Possible contribution from non-cardiomyocyte components in the heart (*e.g.*, fibroblasts, endothelial cells) should not be discounted in TBC1D15-exerted responses in DOX cardiotoxicity. Last but not the least, there is a lack of examination of other TBC1D15 interacting proteins in DOX-challenged hearts.

5. Conclusions

Our findings from our current study noted that *Tbc1d15* ablation protects against DOX-evoked unfavorable changes in cardiac morphology, contractile function, mitochondrial integrity and cell survival through restoration of DNA repair capacity as evidenced by increased DNA-PKcs nuclear translocation. These findings coincide with elevated levels of TBC1D15 in the settings of DOX challenge and human DCM. Our observations should offer new insights towards the clinical treatment of DOX-induced cardiomyopathy. Given the apparent complex and conflicting roles of TBC1D15 in different pathological myocardial stress settings, more in-depth scrutiny is warranted towards a better understanding for the role of TBC1D15 in chronic myopathies. Further study should test the cardiac phenotype in *Tbc1d15* knockout mice replenished with recombinant TBC1D15 to coincide with the *Tbc1d15* knockin findings. Drug development is pertinent in designing small-molecule chemicals targeting TBC1D15. Moreover, genetic information is still lacking connection genetic diseases with TBC family gene mutations to better understand the role of TBC1D15 human health.

Author contributions

Wenjun Yu, Haixia Xu and Zhe Sun were involved in experimental design, data acquisition, analysis, and manuscript preparation. Shiqun Sun, Miyesaier Abudureyimu and Mengjiao Zhang provided technical assistance of echocardiographic measurement. Yuxin Du conducted additional data acquisition and analysis. Jun Tao and Junbo Ge provided necessary resources. Jun Ren and Yingmei Zhang were involved in conception, study design, financial support, supervision and revision of manuscript.

Conflicts of interest

The authors declare no conflicts of interest.

Appendix A. Supporting information

Supporting data to this article can be found online at https://doi.org/10.1016/j.apsb.2023.09.008.

References

1. Gabizon AA, Patil Y, La-Beck NM. New insights and evolving role of pegylated liposomal doxorubicin in cancer therapy. *Drug Resist Updates* 2016;**29**:90−106.
2. Yu J, Wang Y, Zhou S, Li J, Wang J, Chi D, et al. Remote loading paclitaxel-doxorubicin prodrug into liposomes for cancer combination therapy. *Acta Pharm Sin B* 2020;**10**:1730−40.
3. Takemura G, Fujiwara H. Doxorubicin-induced cardiomyopathy from the cardiotoxic mechanisms to management. *Prog Cardiovasc Dis* 2007;**49**:330−52.
4. Shi Y, Moon M, Dawood S, McManus B, Liu PP. Mechanisms and management of doxorubicin cardiotoxicity. *Herz* 2011;**36**:296−305.
5. Wang P, Wang M, Hu Y, Chen J, Cao Y, Liu C, et al. Isorhapontigenin protects against doxorubicin-induced cardiotoxicity *via* increasing YAP1 expression. *Acta Pharm Sin B* 2021;**11**:680−93.
6. Renu K, V Ga, P Bt, Arunachalam S. Molecular mechanism of doxorubicin-induced cardiomyopathy—an update. *Eur J Pharmacol* 2018;**818**:241−53.
7. Zhang S, Liu X, Bawa-Khalfe T, Lu LS, Lyu YL, Liu LF, et al. Identification of the molecular basis of doxorubicin-induced cardiotoxicity. *Nat Med* 2012;**18**:1639−42.
8. Wu L, Wang L, Du Y, Zhang Y, Ren J. Mitochondrial quality control mechanisms as therapeutic targets in doxorubicin-induced cardiotoxicity. *Trends Pharmacol Sci* 2023;**44**:34−49.
9. Kregel S, Bagamasbad P, He S, LaPensee E, Raji Y, Brogley M, et al. Differential modulation of the androgen receptor for prostate cancer therapy depends on the DNA response element. *Nucleic Acids Res* 2020;**48**:4741−55.
10. Suliman HB, Carraway MS, Ali AS, Reynolds CM, Welty-Wolf KE, Piantadosi CA. The CO/HO system reverses inhibition of mitochondrial biogenesis and prevents murine doxorubicin cardiomyopathy. *J Clin Invest* 2007;**117**:3730−41.
11. Lipshultz SE, Grenier MA, Colan SD. Doxorubicin-induced cardiomyopathy. *N Engl J Med* 1999;**340**:653−4. author reply 5.
12. Ichikawa Y, Ghanefar M, Bayeva M, Wu R, Khechaduri A, Naga Prasad SV, et al. Cardiotoxicity of doxorubicin is mediated through mitochondrial iron accumulation. *J Clin Invest* 2014;**124**:617−30.
13. Riad A, Bien S, Gratz M, Escher F, Westermann D, Heimesaat MM, et al. Toll-like receptor-4 deficiency attenuates doxorubicin-induced cardiomyopathy in mice. *Eur J Heart Fail* 2008;**10**:233−43.
14. Li DL, Wang ZV, Ding G, Tan W, Luo X, Criollo A, et al. Doxorubicin blocks cardiomyocyte autophagic flux by inhibiting lysosome acidification. *Circulation* 2016;**133**:1668−87.
15. Guo Q, Guo J, Yang R, Peng H, Zhao J, Li L, et al. Cyclovirobuxine D attenuates doxorubicin-induced cardiomyopathy by suppression of oxidative damage and mitochondrial biogenesis impairment. *Oxid Med Cell Longev* 2015;**2015**:151972.
16. Liu D, Ma Z, Di S, Yang Y, Yang J, Xu L, et al. AMPK/PGC1alpha activation by melatonin attenuates acute doxorubicin cardiotoxicity *via* alleviating mitochondrial oxidative damage and apoptosis. *Free Radic Biol Med* 2018;**129**:59−72.
17. Han D, Wang Y, Wang Y, Dai X, Zhou T, Chen J, et al. The Tumor-suppressive human circular RNA circITCH sponges miR-330-5p to ameliorate doxorubicin-induced cardiotoxicity through upregulating SIRT6, survivin, and SERCA2a. *Circ Res* 2020;**127**:e108−25.
18. Nair RR, Hsu J, Jacob JT, Pineda CM, Hobbs RP, Coulombe PA. A role for keratin 17 during DNA damage response and tumor initiation. *Proc Natl Acad Sci U S A* 2021;**118**:e2020150118.
19. Yoshida M, Shiojima I, Ikeda H, Komuro I. Chronic doxorubicin cardiotoxicity is mediated by oxidative DNA damage−ATM−p53−apoptosis pathway and attenuated by pitavastatin through the inhibition of Rac1 activity. *J Mol Cell Cardiol* 2009;**47**:698−705.
20. Shizukuda Y, Matoba S, Mian OY, Nguyen T, Hwang PM. Targeted disruption of p53 attenuates doxorubicin-induced cardiac toxicity in mice. *Mol Cell Biochem* 2005;**273**:25−32.
21. L'Ecuyer TJ, Aggarwal S, Zhang JP, Van der Heide RS. Effect of hypothermia on doxorubicin-induced cardiac myoblast signaling and cell death. *Cardiovasc Pathol* 2012;**21**:96−104.
22. Blackford AN, Jackson SP. ATM, ATR, and DNA-PK: the trinity at the heart of the DNA damage response. *Mol Cell* 2017;**66**:801−17.
23. Tian X, Seluanov A, Gorbunova V. Beyond making ends meet: DNA-PK, metabolism, and aging. *Cell Metabol* 2017;**25**:991−2.
24. Ihara M, Ashizawa K, Shichijo K, Kudo T. Expression of the DNA-dependent protein kinase catalytic subunit is associated with the radiosensitivity of human thyroid cancer cell lines. *J Radiat Res* 2019;**60**:171−7.
25. Mishra A, Brown AL, Yao X, Yang S, Park SJ, Liu C, et al. Dendritic cells induce Th2-mediated airway inflammatory responses to house dust mite *via* DNA-dependent protein kinase. *Nat Commun* 2015;**6**:6224.
26. Ghonim MA, Pyakurel K, Ju J, Rodriguez PC, Lammi MR, Davis C, et al. DNA-dependent protein kinase inhibition blocks asthma in mice and modulates human endothelial and CD4$^+$ T-cell function without causing severe combined immunodeficiency. *J Allergy Clin Immunol* 2015;**135**:425−40.
27. Park SJ, Gavrilova O, Brown AL, Soto JE, Bremner S, Kim J, et al. DNA-PK promotes the mitochondrial, metabolic, and physical decline that occurs during aging. *Cell Metabol* 2017;**25**:1135−11346.e7.
28. Radhakrishnan SK, Lees-Miller SP. DNA requirements for interaction of the C-terminal region of Ku80 with the DNA-dependent protein kinase catalytic subunit (DNA-PKcs). *DNA Repair* 2017;**57**:17−28.
29. Bartunek J, Vanderheyden M, Knaapen MW, Tack W, Kockx MM, Goethals M. Deoxyribonucleic acid damage/repair proteins are elevated in the failing human myocardium due to idiopathic dilated cardiomyopathy. *J Am Coll Cardiol* 2002;**40**:1097−103. discussion 104−5.
30. Zhou H, Toan S, Zhu P, Wang J, Ren J, Zhang Y. DNA-PKcs promotes cardiac ischemia reperfusion injury through mitigating BI-1-governed mitochondrial homeostasis. *Basic Res Cardiol* 2020;**115**:11.
31. Zhang XM, Walsh B, Mitchell CA, Rowe T. TBC domain family, member 15 is a novel mammalian Rab GTPase-activating protein with substrate preference for Rab7. *Biochem Biophys Res Commun* 2005;**335**:154−61.
32. Wong YC, Ysselstein D, Krainc D. Mitochondria−lysosome contacts regulate mitochondrial fission *via* RAB7 GTP hydrolysis. *Nature* 2018;**554**:382−6.
33. Peng W, Wong YC, Krainc D. Mitochondria−lysosome contacts regulate mitochondrial Ca^{2+} dynamics *via* lysosomal TRPML1. *Proc Natl Acad Sci U S A* 2020;**117**:19266−75.
34. Sun S, Yu W, Xu H, Li C, Zou R, Wu NN, et al. TBC1D15-Drp1 interaction-mediated mitochondrial homeostasis confers cardioprotection against myocardial ischemia/reperfusion injury. *Metabolism* 2022;**134**:155239.
35. Yu W, Sun S, Xu H, Li C, Ren J, Zhang Y. TBC1D15/RAB7-regulated mitochondria−lysosome interaction confers cardioprotection against acute myocardial infarction-induced cardiac injury. *Theranostics* 2020;**10**:11244−63.
36. Kwon D, Park E, Kang SJ. Stimulator of IFN genes-mediated DNA-sensing pathway is suppressed by NLRP3 agonists and regulated by mitofusin 1 and TBC1D15, mitochondrial dynamics mediators. *FASEB J* 2017;**31**:4866−78.
37. Heger J, Hirschhauser C, Bornbaum J, Sydykov A, Dempfle A, Schneider A, et al. Cardiomyocytes-specific deletion of monoamine oxidase B reduces irreversible myocardial ischemia/reperfusion injury. *Free Radic Biol Med* 2021;**165**:14−23.

38. Ortiz-Sanchez P, Villalba-Orero M, Lopez-Olaneta MM, Larrasa-Alonso J, Sanchez-Cabo F, Marti-Gomez C, et al. Loss of SRSF3 in cardiomyocytes leads to decapping of contraction-related mRNAs and severe systolic dysfunction. *Circ Res* 2019;**125**:170−83.

39. Heinen A, Godecke S, Flogel U, Miklos D, Bottermann K, Spychala A, et al. 4-Hydroxytamoxifen does not deteriorate cardiac function in cardiomyocyte-specific MerCreMer transgenic mice. *Basic Res Cardiol* 2021;**116**:8.

40. Ge W, Yuan M, Ceylan AF, Wang X, Ren J. Mitochondrial aldehyde dehydrogenase protects against doxorubicin cardiotoxicity through a transient receptor potential channel vanilloid 1-mediated mechanism. *Biochim Biophys Acta* 2016;**1862**:622−34.

41. Yu W, Gao B, Li N, Wang J, Qiu C, Zhang G, et al. Sirt3 deficiency exacerbates diabetic cardiac dysfunction: role of Foxo3A−Parkin-mediated mitophagy. *Biochim Biophys Acta, Mol Basis Dis* 2017;**1863**:1973−83.

42. Xu H, Yu W, Sun S, Li C, Zhang Y, Ren J. Luteolin attenuates doxorubicin-induced cardiotoxicity through promoting mitochondrial autophagy. *Front Physiol* 2020;**11**:113.

43. Ackers-Johnson M, Li PY, Holmes AP, O'Brien SM, Pavlovic D, Foo RS. A simplified, langendorff-free method for concomitant isolation of viable cardiac myocytes and nonmyocytes from the adult mouse heart. *Circ Res* 2016;**119**:909−20.

44. Xu H, Yu W, Sun S, Li C, Ren J, Zhang Y. TAX1BP1 protects against myocardial infarction-associated cardiac anomalies through inhibition of inflammasomes in a RNF34/MAVS/NLRP3-dependent manner. *Sci Bull* 2021;**66**:1669−83.

45. Zhang Y, Wang C, Zhou J, Sun A, Hueckstaedt LK, Ge J, et al. Complex inhibition of autophagy by mitochondrial aldehyde dehydrogenase shortens lifespan and exacerbates cardiac aging. *Biochim Biophys Acta, Mol Basis Dis* 2017;**1863**:1919−32.

46. Stringer C, Wang T, Michaelos M, Pachitariu M. Cellpose: a generalist algorithm for cellular segmentation. *Nat Methods* 2021;**18**:100−6.

47. Liang X, Wang S, Wang L, Ceylan AF, Ren J, Zhang Y. Mitophagy inhibitor liensinine suppresses doxorubicin-induced cardiotoxicity through inhibition of Drp1-mediated maladaptive mitochondrial fission. *Pharmacol Res* 2020;**157**:104846.

48. Wang S, Tao J, Chen H, Kandadi MR, Sun M, Xu H, et al. Ablation of Akt2 and AMPKalpha2 rescues high fat diet-induced obesity and hepatic steatosis through Parkin-mediated mitophagy. *Acta Pharm Sin B* 2021;**11**:3508−26.

49. Rogakou EP, Boon C, Redon C, Bonner WM. Megabase chromatin domains involved in DNA double-strand breaks *in vivo*. *J Cell Biol* 1999;**146**:905−16.

50. Turinetto V, Giachino C. Multiple facets of histone variant H2AX: a DNA double-strand-break marker with several biological functions. *Nucleic Acids Res* 2015;**43**:2489−98.

51. Ejlerskov P, Rubinsztein DC, Pocock R. IFNB/interferon-β regulates autophagy *via* a *MIR1*−TBC1D15−RAB7 pathway. *Autophagy* 2020;**16**:767−9.

52. Yamano K, Fogel AI, Wang C, van der Bliek AM, Youle RJ. Mitochondrial Rab GAPs govern autophagosome biogenesis during mitophagy. *Elife* 2014;**3**:e01612.

53. Wu L, Sowers JR, Zhang Y, Ren J. Targeting DNA damage response in cardiovascular diseases: from pathophysiology to therapeutic implications. *Cardiovasc Res* 2023;**119**:691−709.

54. Liu X, Chua CC, Gao J, Chen Z, Landy CL, Hamdy R, et al. Pifithrin-alpha protects against doxorubicin-induced apoptosis and acute cardiotoxicity in mice. *Am J Physiol Heart Circ Physiol* 2004;**286**:H933−9.

55. Pan X, Eathiraj S, Munson M, Lambright DG. TBC-domain GAPs for Rab GTPases accelerate GTP hydrolysis by a dual-finger mechanism. *Nature* 2006;**442**:303−6.

56. Bouzakri K, Ribaux P, Tomas A, Parnaud G, Rickenbach K, Halban PA. Rab GTPase-activating protein AS160 is a major downstream effector of protein kinase B/Akt signaling in pancreatic β-cells. *Diabetes* 2008;**57**:1195−204.

57. Stone S, Abkevich V, Russell DL, Riley R, Timms K, Tran T, et al. TBC1D1 is a candidate for a severe obesity gene and evidence for a gene/gene interaction in obesity predisposition. *Hum Mol Genet* 2006;**15**:2709−20.

58. Vizoso M, Ferreira HJ, Lopez-Serra P, Carmona FJ, Martinez-Cardus A, Girotti MR, et al. Epigenetic activation of a cryptic TBC1D16 transcript enhances melanoma progression by targeting EGFR. *Nat Med* 2015;**21**:741−50.

59. Lozano R, Herman K, Rothfuss M, Rieger H, Bayrak-Toydemir P, Aprile D, et al. Clinical intrafamilial variability in lethal familial neonatal seizure disorder caused by TBC1D24 mutations. *Am J Med Genet* 2016;**170**:3207−14.

60. Matsumoto Y, Imai Y, Lu Yoshida N, Sugita Y, Tanaka T, Tsujimoto G, et al. Upregulation of the transcript level of GTPase activating protein KIAA0603 in T cells from patients with atopic dermatitis. *FEBS Lett* 2004;**572**:135−40.

61. Sklan EH, Staschke K, Oakes TM, Elazar M, Winters M, Aroeti B, et al. A Rab-GAP TBC domain protein binds hepatitis C virus NS5A and mediates viral replication. *J Virol* 2007;**81**:11096−105.

62. Wong YC, Peng W, Krainc D. Lysosomal regulation of inter-mitochondrial contact fate and motility in Charcot-Marie-Tooth type 2. *Dev Cell* 2019;**50**:339−354.e4.

63. Cooper A, Garcia M, Petrovas C, Yamamoto T, Koup RA, Nabel GJ. HIV-1 causes CD4 cell death through DNA-dependent protein kinase during viral integration. *Nature* 2013;**498**:376−9.

64. Cao J, Lin G, Gong Y, Pan P, Ma Y, Huang P, et al. DNA-PKcs, a novel functional target of acriflavine, mediates acriflavine's p53-dependent synergistic anti-tumor efficiency with melphalan. *Cancer Lett* 2016;**383**:115−24.

65. Zhou H, Du W, Li Y, Shi C, Hu N, Ma S, et al. Effects of melatonin on fatty liver disease: the role of NR4A1/DNA-PKcs/p53 pathway, mitochondrial fission, and mitophagy. *J Pineal Res* 2018;**64**.

66. Wang Q, Gao F, May WS, Zhang Y, Flagg T, Deng X. Bcl2 negatively regulates DNA double-strand-break repair through a nonhomologous end-joining pathway. *Mol Cell* 2008;**29**:488−98.

67. Fang X, Wang H, Han D, Xie E, Yang X, Wei J, et al. Ferroptosis as a target for protection against cardiomyopathy. *Proc Natl Acad Sci U S A* 2019;**116**:2672−80.

68. Ta N, Qu C, Wu H, Zhang D, Sun T, Li Y, et al. Mitochondrial outer membrane protein FUNDC2 promotes ferroptosis and contributes to doxorubicin-induced cardiomyopathy. *Proc Natl Acad Sci U S A* 2022;**119**:e2217396119.

69. Christidi E, Brunham LR. Regulated cell death pathways in doxorubicin-induced cardiotoxicity. *Cell Death Dis* 2021;**12**:339.